Journal of Environmental Management 397 (2026) 128319

Contents lists available at ScienceDirect

Journal of Environmental Management

journal homepage: www.elsevier.com/locate/jenvman

Review

A comprehensive review on bismuth-based ternary heterojunctions in photocatalytic wastewater treatment

Benjamin O. Orimolade [a,*], Moses G. Peleyeju [b,c], Tunde Lewis Yusuf [a]

[a] Department of Chemistry, Faculty of Natural and Agricultural Sciences, University of Pretoria, Private Bag X20, Hatfield, 0028, Pretoria, South Africa
[b] Department of Biotechnology and Chemistry, Vaal University of Technology, South Africa
[c] Centre for Academic Development, Vaal University of Technology, South Africa

ARTICLE INFO

Keywords:
Ternary heterojunction
Bismuth
Photocatalysis
Wastewater treatment

ABSTRACT

Bismuth-based ternary heterostructured photocatalysts have emerged as one of the most promising classes of materials for wastewater treatment, owing to their narrow band gaps, high structural versatility, and capacity to facilitate efficient charge carrier separation under solar irradiation. Recent studies demonstrate that integrating Bi_2WO_6, $BiVO_4$, BiOX, Bi_2MoO_6, Bi_2O_3, Bi_2S_3, or multi-bismuth phases into ternary configurations, particularly Z-scheme, S-scheme, and dual heterojunction architectures, substantially enhances photocatalytic performance by accelerating interfacial electron transport while preserving strong redox potentials. These systems consistently achieve high degradation efficiencies across dyes, pharmaceuticals, antibiotics, pesticides, and emerging contaminants, frequently outperforming binary and single-component counterparts. Key advances include the use of carbonaceous scaffolds to broaden visible-light absorption, magnetic and transition-metal components to strengthen redox cycling, and defect or vacancy engineering to intensify surface reaction kinetics. Comparative evaluation across recent reports reveals that the most efficient ternary systems often couple broad-spectrum light harvesting with strong built-in electric fields that drive directional charge migration. Despite these advances, persistent challenges remain regarding interfacial stability, secondary pollution risks, and scalability of synthesis routes. Overall, the rapidly evolving evidence indicates that bismuth-based ternary heterostructures represent a highly adaptable, high-performance platform for future solar-driven wastewater treatment, with clear opportunities for optimization through targeted band engineering, green synthesis strategies, and improved photonic utilization.

1. Introduction

Industrial discharge has contaminated water sources worldwide, affecting billions of people who depend on these resources for drinking and agriculture. Manufacturing processes from chemical production, mining operations, electronics fabrication, and petroleum refining release complex mixtures of organic and inorganic contaminants into aquatic environments. The World Health Organization estimates that over 2 billion people lack access to safely managed drinking water, while contaminated water contributes to approximately 3.4 million deaths annually from waterborne diseases (Lee et al., 2023; WHO, UNICEF, World Bank, 2022). Textile industries discharge approximately 200,000 tons of dyes annually into water systems, with synthetic dyes comprising over 60 % of global dye consumption due to their vibrant colors and chemical stability (Oluwasina and Adelodun, 2024; Saini et al., 2025). These aromatic compounds contain chromophoric groups that resist natural degradation processes and accumulate in sediments and aquatic organisms (Alsukaibi, 2022; Ardila-Leal et al., 2021). Pharmaceutical compounds represent an emerging class of micropollutants that appear in surface waters at concentrations ranging from ng/L to μg/L (Jurado et al., 2022; Paíga et al., 2024). Antibiotics, hormones, analgesics, and psychoactive drugs enter water systems through incomplete metabolism in humans and animals, direct disposal of unused medications, and inadequate treatment at pharmaceutical manufacturing facilities. These compounds create persistent threats due to their biological activity and resistance to conventional treatment methods. Studies have detected over 200 different pharmaceutical compounds in drinking water sources across multiple continents, with some showing potential for endocrine disruption and antibiotic resistance development (Khan et al., 2022; Orimolade et al., 2023; Sumpter and Margiotta-Casaluci, 2022). Apart

* Corresponding author.
E-mail address: orimoladeben@yahoo.com (B.O. Orimolade).

https://doi.org/10.1016/j.jenvman.2025.128319
Received 13 September 2025; Received in revised form 6 December 2025; Accepted 10 December 2025
Available online 14 December 2025

from organic pollutants, heavy metals such as chromium, lead, mercury, and cadmium persist indefinitely in aquatic systems due to their non-biodegradable nature (Kurwadkar, 2019; Sharma et al., 2025). Industrial electroplating, metal finishing, and mining activities release these toxic elements at concentrations that exceed regulatory limits in many regions. Even low concentrations can bioaccumulate through food chains, causing neurological damage, kidney dysfunction, and developmental disorders in exposed populations (Akter et al., 2020; Nkinda et al., 2021).

Traditional wastewater treatment plants achieve less than 50 % removal efficiency for many synthetic organic pollutants and pharmaceutical residues because they were designed primarily for biological oxygen demand reduction and pathogen removal but not chemically stable compounds with complex molecular structures (Arman et al., 2021; Karpińska and Kotowska, 2019; Sathya et al., 2022). For example, the sedimentation tank of a conventional wastewater treatment plant was reported to remove only 30 % of polycyclic aromatic hydrocarbons and caffeine (Ozaki et al., 2025). Similarly, aerobic biological process in activated sludge achieved 24–40 % removal of pyrazines, a core component of many pharmaceuticals (Macêdo et al., 2025). Also, the removal of diclofenac using a conventional constructed wetland (which depends on adsorption, biodegradation and plant uptake) achieved only 48 % (Ofiera et al., 2025). Advanced treatment technologies such as membrane filtration and activated carbon adsorption can improve removal efficiency but generate concentrated waste streams that require further treatment and disposal (Bera et al., 2022; Lotfy and Roubík, 2023).

Photocatalytic degradation offers a different approach to address these limitations. While conventional methods cannot remove recalcitrant organics completely and some advanced methods such as membrane filtration merely transfer contaminants between phases, photocatalysis can completely mineralize organic pollutants into harmless CO_2 and H_2O through light-driven redox reactions (Som et al., 2020). Single-component photocatalysts face significant obstacles. For example, TiO_2, which is the most reported photocatalyst, absorbs only 4 % of solar radiation due to its wide bandgap of 3.2 eV (Yazhou Wang et al., 2020). Visible light active alternatives often suffer from poor stability or rapid charge recombination rates that exceed 10^{-9} s. Heterostructured photocatalysts overcome these fundamental limitations through new design approaches. Binary heterojunctions showed initial promise, but ternary systems have demonstrated superior capabilities. These three-component architectures create multiple charge transfer pathways and extend carrier lifetimes to microsecond ranges while maintaining strong oxidative potentials. Ternary systems often exceed the sum of individual components, with some studies reporting degradation rates 5 to 10 times higher than binary counterparts.

Bismuth-based semiconductors have attracted attention due to their electronic properties and environmental compatibility. The $6s^2$ lone pair electrons in bismuth create hybridized valence bands that narrow the bandgap to the visible region between 1.7 and 2.8 eV while maintaining suitable band edge positions for water oxidation and organic pollutant degradation. Compounds such as $BiVO_4$, Bi_2WO_6, and bismuth oxyhalides (BiOX) demonstrate stability under operational conditions. This provides advantages over sulfide-based photocatalysts that suffer from photocorrosion. Incorporating bismuth-based semiconductors into ternary heterostructures has produced notable results. Recent studies report near complete degradation of persistent pollutants such as ciprofloxacin, methylene blue, and phenols within 60–120 min under visible light (Guo et al., 2020; Shen et al., 2023; J. Wang et al., 2021). These systems utilize charge separation mechanisms, including Z-scheme and S-scheme pathways that preserve high redox potentials while extending charge carrier lifetimes. While significant progress has been made in developing bismuth-based ternary heterostructured photocatalysts, their practical relevance to real wastewater environments is often underrepresented in many discussions. Many bismuth-based ternary systems exhibit high oxidative capability, rapid charge separation, and broad-spectrum light harvesting, which enable them to operate effectively under variable pH, high ionic strength, and the presence of natural organic matter (Alomayri, 2025; Tahir et al., 2022; Z. xu Wang et al., 2025). More importantly, their structural robustness and tunable morphologies facilitate resistance to radical scavenging, decreased catalyst deactivation, and improved recyclability, making them well suited for real wastewater where multiple competing species coexist. Emerging studies have also integrated these photocatalysts into membrane reactors, photo-Fenton hybrid systems, composite sponges, and flow-through configurations, highlighting their potential for scalable deployment (B. Gao et al., 2022b; Xie et al., 2022, 2021). However, the translation from controlled aqueous systems to practical wastewater treatment remains limited, and a clearer understanding of how these materials perform under realistic operating conditions is required.

Nevertheless, the field lacks a comprehensive analysis specifically focused on bismuth-based ternary photocatalysts for environmental remediation despite growing research interest. Existing reviews either broadly cover ternary photocatalyst without material-specific insights or focus on bismuth compounds without adequate attention to their ternary architectures (Ben Saber et al., 2020; Mohana Roopan and Khan, 2023; Orimolade and Arotiba, 2020; Zulfa et al., 2024). This knowledge gap limits the rational design of improved photocatalysts and impedes technology transfer to practical applications. This review provides a comprehensive and mechanistic synthesis of bismuth-based ternary heterostructured photocatalysts for pollutant degradation. We evaluate how band-structure engineering, interfacial charge dynamics, and morphology-dependent design collectively determine photocatalytic performance, while also assessing environmental safety, recyclability, and fabrication feasibility. By integrating these dimensions, the review establishes a clearer framework for the rational design of next-generation bismuth-based ternary photocatalysts and outlines the emerging trends that will shape their translation toward practical water treatment technologies.

2. Fundamentals of heterogeneous photocatalysis and ternary heterojunctions

Heterogeneous photocatalysis involves the light-induced catalytic transformation of pollutants using semiconducting materials. When a semiconductor absorbs photons of sufficient energy, electrons move from the valence band to the conduction band, creating positive holes in the valence band. These charge carriers migrate to the catalyst surface and drive redox reactions with adsorbed molecules. Electrons reduce oxygen molecules into superoxide radicals, while holes oxidize water or hydroxyl ions into hydroxyl radicals. These reactive oxygen species nonselectively attack and degrade various pollutants, including dyes, pharmaceuticals, phenols, and heavy metals (Fujishima et al., 2008; Kanakaraju et al., 2018; Maynez-Navarro and Sánchez-Salas, 2018). The practical efficiency of photocatalysis faces several limitations. Wide bandgap semiconductors absorb insufficient visible light, which restricts their application to only UV radiation. Another challenge is that photoinduced electrons and holes recombine rapidly (Morshedy et al., 2024; H. Wang et al., 2022). Catalysts often show poor selectivity or stability under operating conditions. These problems are particularly evident in single-phase semiconductors.

Heterojunction engineering addresses these challenges by coupling two or more semiconductors with different band structures, which results in band alignment at their interfaces (Wang et al., 2014). These interfaces favour charge separation and extend the spectral response into the visible range. Several heterojunction architectures exist, each with distinct charge transfer mechanisms. For instance, the Type II heterojunctions facilitate stepwise migration of photogenerated electrons and holes across the interface. Electrons migrate from the conduction band of the narrow bandgap semiconductor to the conduction band of the wide bandgap material while photogenerated holes move in the opposite direction (Low et al., 2017; Zhang and Jaroniec, 2018). This

promotes spatial separation but often compromises redox power due to energy losses at the interface. Z-scheme heterojunctions follow natural photosynthesis principles and allow only the most energetic charge carriers to participate in redox reactions. Electrons in the conduction band of one semiconductor recombine with holes in the valence band of another semiconductor (Xu et al., 2018). This process leaves behind electrons with high reducing power and holes with strong oxidizing ability in their respective bands. The configuration combines strong redox activity with spatial separation. S-scheme heterojunctions represent a newer variant of the Z-scheme. Internal electric fields, band bending, and Fermi level equilibration guide charge separation along energetically favorable pathways (Nie et al., 2024; L. Wang et al., 2022). These systems appear increasingly in bismuth-based ternary photocatalysts. Junction types based on charge carrier differences also exist. p-n junctions rely on electrostatic fields created at the junction of materials with different majority charge carriers. This field promotes directional separation of charges while n-n or p-p systems require appropriate band offsets for efficient interfacial electron migration (Low et al., 2017).

Ternary heterojunction systems expand the design space and functional diversity by introducing a third component. The third component can serve multiple roles. It may act as an electron mediator that enhances interfacial conductivity, such as MXene or graphene materials. It can function as a photosensitizer that extends light absorption into the visible or near infrared range, like quantum dots. The component might serve as a redox co-catalyst that lowers activation barriers, including noble metals. Finally, it may act as a structural stabilizer that prevents agglomeration and ensures long-term photocatalytic durability (Balapure et al., 2024; Kausar et al., 2022; Mohana Roopan and Khan, 2023). Ternary systems enable dual Z-scheme, S-scheme, or cascade-type band alignments. Photogenerated charges follow multistep paths that minimize recombination while preserving redox potential. The arrangement of components, interface quality, and contact mode all influence the final photocatalytic performance. Contact modes include core-shell, layered, and porous configurations (Cai et al., 2024; Ji et al., 2024; Liang et al., 2022).

Bismuth-based semiconductors prove especially valuable in ternary systems. $BiVO_4$, Bi_2WO_6, BiOI, BiOBr, and Bi_2MoO_6 possess narrow band gaps and high visible light response. They form layered structures that facilitate charge transport. Their electronic structures enable strong oxidizing or reducing capabilities depending on band alignment. Many bismuth oxyhalides possess internal electric fields due to asymmetric crystal structures. These fields aid in the separation of charge carriers. Bismuth-based materials have limitations, including poor stability under acidic or alkaline conditions and susceptibility to photo corrosion. Ternary architectures address these issues by integrating stabilizing components and optimizing interface design. These systems offer enhanced light utilization, improved separation of photogenerated carriers, greater stability, and superior pollutant degradation efficiency. The following sections examine ternary composites that incorporate bismuth-based semiconductors, focusing on their roles, configurations, degradation mechanisms, and practical applications in pollutant removal.

3. Bismuth-based ternary heterostructures for the removal of pollutants

Bismuth-based semiconductors have attracted growing interest in photocatalysis owing to their tunable band structures, chemical versatility, and visible-light responsiveness. These materials often serve as the backbone of heterostructured photocatalysts due to their unique electronic configurations and ability to form stable, layered, or anisotropic structures that promote effective charge separation. Within ternary composites, bismuth-based materials typically function as either light absorbers or charge transfer mediators, depending on their energy band alignment and structural compatibility with other constituents. As shown in Fig. 1, prominent bismuth materials that have been incorporated in ternary heterojunctions include $BiVO_4$, Bi_2WO_6, Bi_2S_3, Bi_2O_3, and bismuth halides (BiOI, BiOCl, and BiOBr). Other less common bismuth compound semiconductors have also been reported to have good performance in ternary heterostructures.

3.1. Bi_2WO_6-based ternary heterojunctions

The layered Aurivillius-type structure of Bi_2WO_6, combined with its suitable bandgap (~2.8 eV) and oxidative capability, makes it a strong candidate for visible-light photocatalysis (Finlayson et al., 2006; Li et al., 2008; Orimolade et al., 2021). However, its relatively poor charge mobility and electron–hole recombination necessitate structural modification. Integration into ternary heterojunctions has proven to be an effective strategy for improving its photocatalytic performance, and it is often paired with 2D materials or redox-active co-catalysts. These ternary systems are often engineered to form Z-scheme, S-scheme, or Schottky-type interfaces that enhance charge separation and broaden visible light utilization.

In the construction of ternary heterojunctions, carbon-based materials such as graphene oxides are common components. This is because of their good conductivity owing to many conjugated π bonds and a 2D sheet structure. When incorporated into heterojunctions, GO acts as mediator responsible for charge transportation of photogenerated electrons which limits the severity of recombination of photogenerated holes with electrons. Also, its huge specific surface area due to its 2D sheet structure is beneficial for improved photocatalytic performance. Several reports have explored the synergistic role of GO and Bi_2WO_6 in ternary heterojunction photocatalysts. For example, a composite photocatalyst consisting of AgBr/GO/Bi_2WO_6 with a ternary heterojunction has been constructed and applied for the photocatalytic removal of tetracycline hydrochloride (Guan et al., 2021). In this study, a binary heterojunction of GO and Bi_2WO_6 was first prepared through hydrothermal synthesis. To obtain the ternary heterojunction consisting of AgBr, in-situ deposition was employed. The prepared GO/Bi_2WO_6 was dispersed in deionized water, subjected to ultrasound treatment in the dark and then corresponding amounts of $AgNO_3$ and KBr salts were added to the GO/Bi_2WO_6 solution under continuous stirring. Hence, the final ternary composite was achieved at an ambient temperature using a simple approach. The presence of GO provided a conductive scaffold that enhanced charge carrier mobility, while AgBr acted as a visible-light photosensitizer and reactive site. The ternary system showed high efficiency in tetracycline degradation driven by a Z-scheme mechanism that enabled strong redox potentials. Specifically, 84 % removal was recorded with the ternary photocatalyst, which was more than four times and three times higher than that of AgBr and Bi_2WO_6,

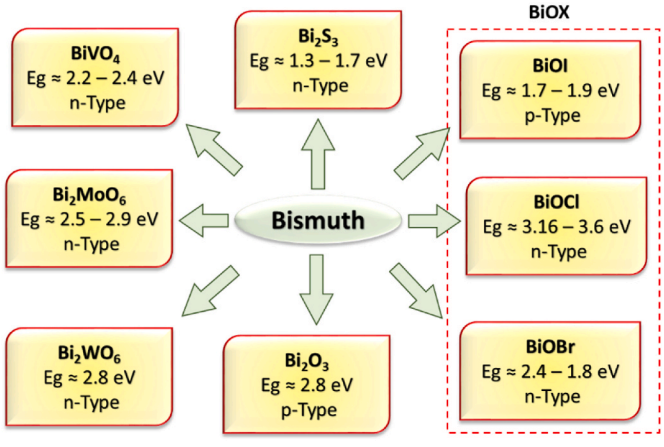

Fig. 1. Bismuth based compounds common in ternary heterostructures and their band gap energies.

respectively. In a related study involving GO and Bi_2WO_6 in a ternary composite, Hu et al. synthesized a ternary Z-scheme system comprising Bi_2WO_6, rGO, and meso-tetra(4-carboxyphenyl) porphyrin (TCPP) (Hu et al., 2019). The hydrothermal synthesis route was also employed for the preparation of rGO/Bi_2WO_6, which was subsequently combined with TCPP through the liquid ultrasonic route. In this case, the after adding TTCP to the suspension of rGO/Bi_2WO_6, the mixture was subjected to both ultrasound treatment and continuous stirring at ambient temperature. The constructed ternary heterostructured displayed improved photocatalytic efficiency, which resulted from the synergistic effect of rGO and TCPP in conjunction with Bi_2WO_6. The rGO improved interfacial conductivity while TCPP broadened the light absorption range of the ternary composite. The recombination of photoinduced electron hole pairs in the Bi_2WO_6 was remarkably suppressed possibly through a Z-scheme mechanism, resulting in 79.27 % removal of tetracycline within 60 min. Also, the catalyst demonstrated a good stability with a minimal loss of approximately 4 % degradation efficiency after five repeated use and no observable change in its morphology. Evidently, Bi_2WO_6-based ternary photocatalysts consisting of GO offer good photocatalytic performances and are effective for the degradation of pharmaceuticals such as antibiotics in wastewater.

Furthermore, Xie et al. constructed a porous TiO_2–Bi_2WO_6 composite anchored on graphene oxide, forming a three-dimensional architecture that provided abundant active sites for ethylene degradation under visible light (Xie et al., 2021). The composite photocatalyst was constructed through hydrothermal and surface-deposition methods. The surface-deposition was also carried out by subjecting a mixture of hydrothermally prepared TiO_2-Bi_2WO_6 and graphene oxide to ultrasonic treatment for 30 min. Apart from the fact that GO acted as a good mediator for charge transport in the ternary heterojunction, the presence of Bi_2WO_6 made the photocatalyst visible light responsive, unlike pristine TiO_2. Importantly, the plausible mechanism proposed from the results of UV–Vis spectroscopy band gap energy measurement and quenching test suggests that efficient charge separation was promoted in the composite catalyst through a staggered Type II heterojunction whereby the holes in the valence band of Bi_2WO_6 to the valence band of TiO_2, while the photogenerated electrons in the conduction band of TiO_2 migrated to the conduction band of Bi_2WO_6 (Fig. 2a). This efficient charge separation led to enhanced photocatalytic degradation of ethylene. The apparent rate constant using the ternary composite was 0.0013 $min^{-1,}$ which was fifteen times higher than that of TiO_2 and twice that of Bi_2WO_6. Such improved performance was also recorded in the application of ternary heterostructured Au@TiO_2/Bi_2WO_6 in the photocatalytic removal of antibiotics under visible light (Jin et al., 2022). However, as shown in Fig. 2b, the authors proposed a Z-scheme charge separation whereby the Au acted as electron mediator in which the electrons from the conduction band of TiO_2 recombined with the holes from the valence band of Bi_2WO_6. This resulted in efficient charge separation within both Bi_2WO_6 and TiO_2. The reactive species form from the well separated charge carriers then oxidized the antibiotic molecules. However, the proposed mechanism was not confirmed through more accurate techniques such as in-situ XPS or density functional theory analyses. Nevertheless, the catalyst show good stability after four cycle experiments and has potential wastewater treatment.

Graphitic carbon nitride (g-C_3N_4), a metal-free semiconductor, is another common component of Bi_2WO_6 based ternary heterostructured photocatalyst. The use of g-C_3N_4 is attractive because of its good optical properties, thermal and chemical stability. For example, Mirhosseini et al. fabricated a TiO_2/Bi_2WO_6/g-C_3N_4 composite using a facile approach and applied it for the removal of brilliant green dye (Mirhosseini et al., 2022). In this system, both g-C_3N_4 and Bi_2WO_6 served as a visible-light absorber. Charge separation was promoted in the ternary heterojunctions through the migration of photogenerated charge carriers across the three semiconductors. Electrons in the conduction band of g-C_3N_4 moved to the conduction band of Bi_2WO_6 through the conduction band of TiO_2. Holes are retained in the valence band of g-C_3N_4, which produced hydroxyl radicals. This system, with improved separation of electrons and holes, resulted in enhanced photodegradation of the dye molecules, achieving 99.92 % removal within 70 min. In another recent study involving g-C_3N_4 and Bi_2WO_6, the third component in the ternary heterojunction was an organic metal organic framework (MOF), MIL-100 (Fe) (Peyrovi et al., 2025). Generally, MOFs possess fascinating features such as high pore volume and surface area, unsaturated metal sites, and tunable porous structures (Xu et al., 2024). The MIL-100(Fe)@Bi_2WO_6/g-C_3N_4 photocatalyst was synthesized using the hydrothermal synthesis route, whereby a specific amount of prepared Bi_2WO_6/g-C_3N_4 was dispersed in the precursor solution of MIL-100(Fe). Efficient charge separation was achieved in the composite possibly through a dual Z-scheme heterojunction, where the photogenerated electrons of Bi_2WO_6 combined with the holes of g-C_3N_4 (Fig. 2c). This resulted in improved removal of Reactive Blue 4 dye, attaining 94 % within 2 h.

While expanding the scope of ternary heterostructures for wastewater treatment, Subhiskha et al. constructed $CuWO_4$/Bi_2WO_6/MnS photocatalyst for the removal of both phenolic compounds and heavy metals from polluted water (Subhiksha et al., 2022). This ternary composite consisting of a dual heterojunction is unique in that all the component semiconductors are visible light responsive. The ternary composite was synthesized through the co-precipitation method and an ultrasonication-assisted route. The measured band gap energy of the composite was 2.4 eV, which was lower than that of the individual constituents, suggesting improved visible-light absorption and better photoactivity. As envisaged, the $CuWO_4$/Bi_2WO_6/MnS achieved improved photocatalytic degradation of 4-chlorophenol and chromium (VI) with 99.8 % and 97 % removal, respectively. These values were more than twice what was recorded with the pristine semiconductors and binary systems. The enhanced performance of the ternary composite was ascribed to the formation of a dual heterojunction between the semiconductors, whereby a type-II heterojunction was formed between Bi_2WO_6 and MnS, while a type-I heterojunction was formed between $CuWO_4$ and Bi_2WO_6, which greatly impeded the recombination of the photoinduced charge carriers. Importantly, too, the toxicity of the ternary photocatalytic system was evaluated, and the composite was found to be non-toxic to *Allium cepa*. This confirmed the sustainability of using Bi_2WO_6-based ternary heterojunction for wastewater treatment without the danger of secondary pollutants. In other studies, polymeric materials have been adopted in Bi_2WO_6-based ternary photocatalysts, and this offers other functionality such as coupling membrane filtration with photocatalysis (Asadpoor et al., 2025; H. Wang et al., 2020; Xie et al., 2022).

These diverse studies illustrate the effectiveness of ternary architectures in enhancing the performance of Bi_2WO_6-based photocatalysts. Whether constructed with carbon materials, visible-light semiconductors, noble metals, or polymers, the common strategy lies in engineering interfaces that maximize light absorption, promote spatial charge separation, and sustain strong redox potentials. The configuration of heterojunctions particularly Z-scheme and Type-II hybrids proved central in unlocking the full potential of Bi_2WO_6 for visible-light-driven degradation of a wide range of pollutants.

3.2. $BiVO_4$-based heterojunctions

Among visible-light-active photocatalysts, $BiVO_4$ remains a frontrunner due to its moderate bandgap (~2.4 eV), stable scheelite structure, and high oxidative potential (Kim and Lee, 2019; Tayebi and Lee, 2019; Z. Wang et al., 2019). It is also non-toxic with good chemical stability. Yet, its use in real photocatalytic applications is constrained by sluggish electron transport and fast charge recombination (Ma et al., 2025). To resolve these issues, $BiVO_4$ has been widely integrated into ternary heterojunctions with other semiconductors and functional materials. These systems are typically constructed in Z-scheme or dual Z-scheme configurations, where photogenerated electrons and holes are

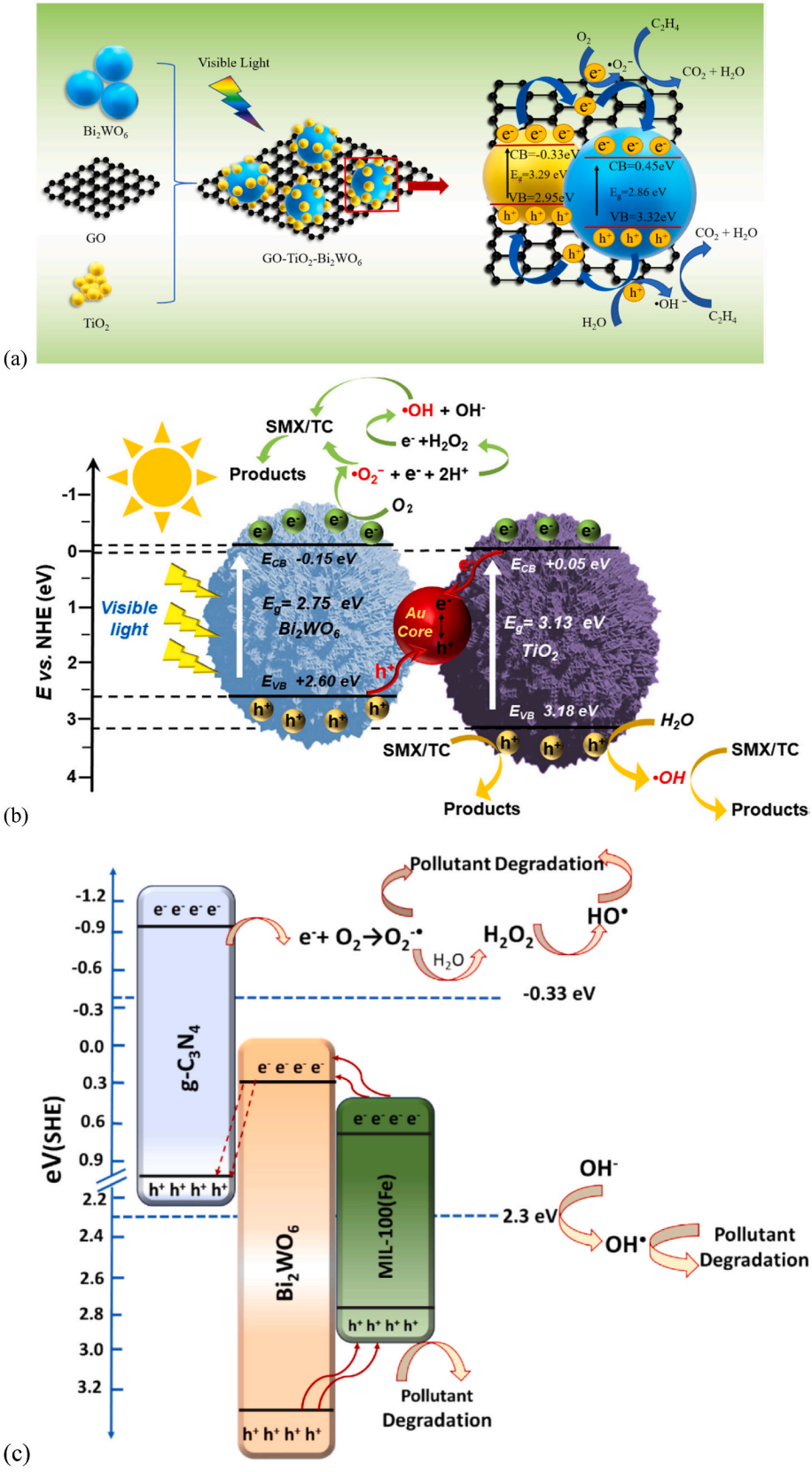

Fig. 2. (a) Plausible mechanism of charge separation in type II heterojunction of GO-TiO_2/Bi_2WO_6 (Reproduced with permission from Ref (Xie et al., 2021) Copyright Elsevier 2021) (b) Probable synergistic separation and electron transfer mechanism for the Z-scheme heterostructure of Au@TiO_2/Bi_2WO_6 nanocomposite (Reproduced with permission from Ref (Jin et al., 2022) Copyright Elsevier 2022) (c) Plausible mechanism of charge separation in MIL-100(Fe)@Bi_2WO_6/g-C_3N_4 (Reproduced with permission from Ref (Peyrovi et al., 2025) Copyright Elsevier 2025).

separated across discrete interfaces, thus preserving strong redox potentials while suppressing recombination losses. Notably, a combination of band alignment engineering, interfacial contact control, and conductive pathways defines the design of efficient $BiVO_4$-based ternary systems.

A significant breakthrough in bismuth-based ternary photocatalysts with dual Z-scheme architecture has been reported. For example, Wang et al. synthesized an AgI/$ZnIn_2S_4$/$BiVO_4$ ternary photocatalyst with a dual Z-scheme separation mechanism and applied it for the degradation of tetracycline antibiotics (S. Wang et al., 2022). The composite photocatalyst was synthesized via a sequential hydrothermal and in-situ precipitation method. First, $ZnIn_2S_4$ was synthesized using a hydrothermal route using zinc acetate, indium nitrate, and thioacetamide. The $ZnIn_2S_4$ was then combined with bismuth nitrate and ammonium vanadate solutions and hydrothermally treated at 180 °C for 24 h to form $ZnIn_2S_4$/$BiVO_4$. Finally, AgI was deposited through coprecipitation by mixing the composite with $AgNO_3$ and KI solutions in the dark. Photoluminescence (PL) spectra and transient photocurrent responses confirmed reduced electron–hole recombination, validating the proposed charge separation mechanism. The proposed mechanism showed that one Z-scheme heterojunction was formed between $BiVO_4$ and AgI, while another was formed between AgI and $ZnIn_2S_4$. This dual Z-scheme enabled directional charge recombination at AgI, allowing high-energy electrons from $ZnIn_2S_4$ and holes from $BiVO_4$ to remain active for redox reactions. As a result, the composite achieved 91.44 % degradation of tetracycline in 2 h under visible light. Interestingly, the photocatalyst still demonstrated good efficiency after ten cycle experiments with a reduction of 9 % in degradation efficiency. However, the morphology and structure were not assessed after use. This is essential to ascertain the integrity of the material for real wastewater treatment.

Similar $ZnIn_2S_4$–$BiVO_4$ pairing was also investigated by Zhang et al., where a core-shell $BiVO_4$@$ZnIn_2S_4$/$Bi_2Sn_2O_7$ ternary photocatalyst was constructed (Zhang et al., 2021). To achieve the successful preparation of the composite, a hydrothermal and heat-circumfluence synthesis strategy was adopted. $BiVO_4$ truncated octahedrons were prepared via a solid-liquid reaction and coated with $ZnIn_2S_4$ nanosheets to form core-shell structures. $Bi_2Sn_2O_7$ nanoparticles were hydrothermally synthesized and then anchored onto the $ZnIn_2S_4$ surface, yielding the ternary $BiVO_4$@$ZnIn_2S_4$/$Bi_2Sn_2O_7$ heterojunction. The resulting dual Z-scheme heterostructure possessed a large oxidation surface and strong oxidation ability. This was due to the proposed enhanced charge separation as shown in Fig. 3. When irradiated with visible light, the excited electrons in both the $Bi_2Sn_2O_7$ and $BiVO_4$ combined with the photogenerated holes in $ZnIn_2S_4$. This allowed well-separated photogenerated holes in $Bi_2Sn_2O_7$ and $BiVO_4$ to facilitate fast photocatalytic activity. This strategy led to about 81 % degradation of Rhodamine B in 60 min, and the system retained its activity after five cycles. More remarkable is the fact that the apparent rate constant values obtained showed that the photocatalytic degradation process was around 63 and 12 times faster than that of pristine $BiVO_4$ and $Bi_2Sn_2O_7$. Evidently, bismuth-based dual Z-scheme heterojunctions have great potential for wastewater treatment.

While Z-scheme systems built on narrow bandgap sulfides have been effective, carbonaceous materials like graphene offer additional pathways to enhance photocatalytic performance through improved conductivity and interfacial charge transport. In this regard, Alomayri et al. prepared a $BiVO_4$/rGO/$FeVO_4$ ternary heterojunction using a hydrothermal method (Alomayri, 2025). The rGO nanosheets served as a conductive bridge between $BiVO_4$ and $FeVO_4$, facilitating Z-scheme band alignment. At the same time, the rGO caused more active agent sites and enhanced surface area, which increased the light absorption capacity. This system achieved 99.52 % degradation of methyl orange within 60 min, and photophysical studies confirmed efficient carrier migration and minimal recombination. The incorporation of rGO also imparted mechanical stability and reusability over multiple cycles.

Incorporating noble metals into $BiVO_4$-based ternary composites has proven to be another effective strategy for enhancing interfacial charge dynamics and photocatalytic efficiency. Gao et al. successfully synthesized a hierarchically structured {010}$BiVO_4$/Ag/CdS Z-scheme photocatalyst through a sequential deposition method (B. Gao et al., 2022a). The $BiVO_4$ component, enriched with high-energy {010} facets, was first fabricated hydrothermally with $TiCl_3$ modulation to increase the exposure of reactive planes. Ag nanoparticles were subsequently introduced via photoreduction of $AgNO_3$, selectively anchoring onto the reduction-favored {010} facets. This was followed by uniform chemical deposition of CdS nanoparticles through precipitation. The resulting ternary Z-scheme heterojunction featured Ag as an electron mediator, which facilitated efficient charge transfer between CdS and $BiVO_4$, suppressed electron-hole recombination, and preserved strong redox potentials. The composite demonstrated remarkable photocatalytic activity, achieving over 98 % removal of fluoroquinolone antibiotics in water within 50 min under visible light. The localized surface plasmon resonance (LSPR) effect of Ag broadened the visible-light absorption, while electron paramagnetic resonance (EPR) analyses confirmed that holes and superoxide radicals were the dominant reactive species driving the degradation process. These results underscore the

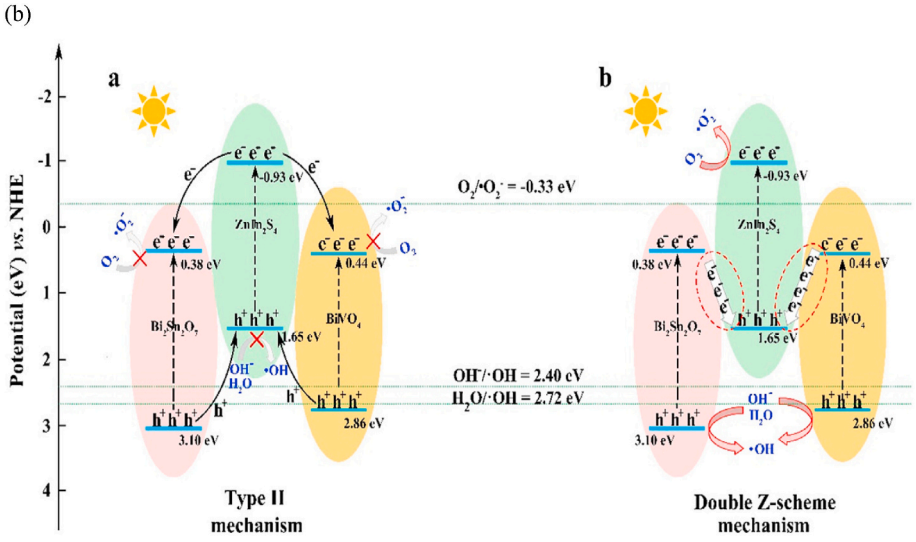

Fig. 3. (a) Schematic diagram for the possible charge separation of $BiVO_4$@$ZnIn_2S_4$/$Bi_2Sn_2O_7$ ternary heterojunction (a: type II; b: double Z-scheme). (Reproduced with permission from Ref (Zhang et al., 2021) Copyright Elsevier 2021).

effectiveness of combining facet-engineered $BiVO_4$ with plasmonic metals and narrow-bandgap semiconductors to construct high-performance photocatalytic systems for water treatment applications.

Further expanding the diversity of ternary composites, Wang et al. (2020) constructed a Co_3O_4–$BiVO_4$/g-C_3N_4 composite using thermal polymerization and hydrothermal growth (Yile Wang et al., 2020). g-C_3N_4 was synthesized by calcining melamine, Co_3O_4 via urea-assisted hydrothermal growth, and the final heterostructure was annealed to establish interfacial bonds. The p–n–n configuration created built-in electric fields and facilitated spatial separation of electrons and holes. The authors proposed a direct dual Z-scheme interface which allowed holes in Co_3O_4 and electrons in g-C_3N_4 to participate in redox processes, while $BiVO_4$ acted as a central recombination site. This suggested mechanism was supported with results from electron spin spectroscopy (ESR) measurement, scavenging test and PL analyses. The photocatalyst degraded >95 % of methylene blue within 60 min, and photocurrent studies supported the effective charge migration pathway. The large surface area of the photocatalysts due to coral flake-like structure contributed to its performance. Additionally, the photocatalyst showed good stability after five cycles with no detectable change in its structure and morphology while degradation efficiency dropped by only 5 % demonstrating potential for wastewater treatment.

A more biologically oriented design was reported by Athar and Muneer, who constructed a GO-stimulated In_2O_3/$BiVO_4$ Z-scheme photocatalyst using in situ hydrothermal assembly (Athar and Muneer, 2024). $BiVO_4$ and In_2O_3 nanoparticles were grown on graphene oxide nanosheets, ensuring a high degree of dispersion and interfacial contact. This composite demonstrated >90 % degradation of methylene blue and ciprofloxacin under visible light, and uniquely, it showed anticancer and toxicity reduction activity in simulated effluent water. The Z-scheme heterostructure facilitated strong redox reactions, while GO contributed to electron delocalization, enhancing charge mobility. This study highlighted the potential for $BiVO_4$-based ternary systems to bridge environmental and biomedical applications.

These studies demonstrate various synthetic approaches and structural designs for creating $BiVO_4$-based ternary heterojunctions. The different methods, including incorporating noble metals, using rGO frameworks, or combining dual-sulfide materials, all work toward the same goal: improving photocatalytic performance by better separating interfacial charges and extending carrier lifetimes. The synthesis technique chosen (hydrothermal, sol-gel, photoreduction, or polymeric calcination) depends on how well materials work together and the specific charge transfer pathways needed. Most systems achieve impressive results, with degradation efficiencies exceeding 90 %, maintain good structural integrity, and provide clear understanding of their mechanisms. This confirms that $BiVO_4$ remains a valuable foundation for developing advanced photocatalysts.

3.3. BiOX-based ternary heterojunctions

The bismuth oxyhalide family, BiOX (X = Cl, Br, I), offers an appealing class of layered semiconductors characterized by a unique internal electric field arising from their $[Bi_2O_2]^{2+}$ slabs interleaved with halide layers (Huang and Zhu, 2009; Hussain et al., 2024; Zhang et al., 2024). Among them, BiOBr and BiOI have drawn significant attention due to their narrower band gaps and stronger visible light absorption compared to BiOCl. However, like many single-component semiconductors, pristine BiOX materials suffer from rapid recombination of photogenerated electron–hole pairs and limited redox ability when used alone. The strategic integration of BiOX with complementary semiconductors in ternary heterojunctions has emerged as a powerful route to mitigate these shortcomings. In these systems, rational band alignment enables directional charge migration, while conductive scaffolds or magnetic components often contribute to enhanced charge mobility and reusability. Below, notable ternary systems are discussed, showcasing design rationale, synthesis methods, degradation performance, and underlying photocatalytic mechanisms.

A notable example of BiOX-based ternary heterostructure is the ternary 2D/2D AgBr/g-C_3N_4/BiOBr composite developed by Tang et al. (2019). The material was synthesized using a combination of hydrothermal synthesis and ion-exchange approach. Firstly, prepared g-C_3N_4 was added to the precursor solution for BiOBr and hydrothermally treated at 120 °C for 24 h to obtain binary g-C_3N_4/BiOBr nanosheets. Thereafter, $AgNO_3$ was added dropwise to the ethylene glycol solution containing g-C_3N_4/BiOBr and then aged for 2 h in the dark to obtain AgBr/g-C_3N_4/BiOBr ternary heterostructured nanosheets. The nanosheet configuration facilitated intimate contact between components, allowing effective interfacial charge transfer. The proposed charge separation was two-step type-II heterojunction due to the band alignment of the three semiconductors as shown in Fig. 4a where the photogenerated electrons from g-C_3N_4 transferred to the conduction band of AgBr and finally to the conduction band of BiOBr while all the holes are were transferred into the valence band of g-C_3N_4. Consequently, under visible light irradiation, the system achieved significant removal of organic dye and antibiotics, with 98 % and 78.2 % degradation of rhodamine B and tetracycline, respectively, in 60 min.

In a related design emphasizing electron mobility, Chen et al. introduced carbon quantum dots (CQDs) into a BiOBr/g-C_3N_4 system via hydrothermal decoration (Chen et al., 2024). The CQDs acted as a conductive interlayer and a visible-light sensitizer, bridging charge transport across BiOBr and g-C_3N_4. The ternary composite achieved over 99.63 % degradation of tetracycline hydrochloride within 50 min and 100 % in 60 min, outperforming binary BiOBr/g-C_3N_4. PL and time-resolved photoluminescence studies confirmed suppressed charge recombination and longer lifetimes of photogenerated electrons. The authors proposed a CQD-enhanced Z-scheme mechanism, where electrons are transferred from the conduction band of BiOBr through the CQDs instead of recombining directly, thereby enhancing charge carrier utilization. Additionally, CQDs possess a distinct π-π conjugated structure that also contributed to the separation of the photogenerated electron-hole pairs in the BiOBr. Evidently, CQDs are suitable materials for enhancing the performance of BiOX-based ternary heterostructures.

In other studies, involving BiOX ternary heterostructures, magnetic recovery, which is a practical need in photocatalysis, has been introduced using ferrite components. For example, Jiang et al. constructed a magnetically recoverable flower-like AgBr/BiOBr/$NiFe_2O_4$ heterojunction with enhanced visible light activity (Jiang et al., 2022). BiOBr was synthesized first and combined with AgBr nanoparticles via in situ

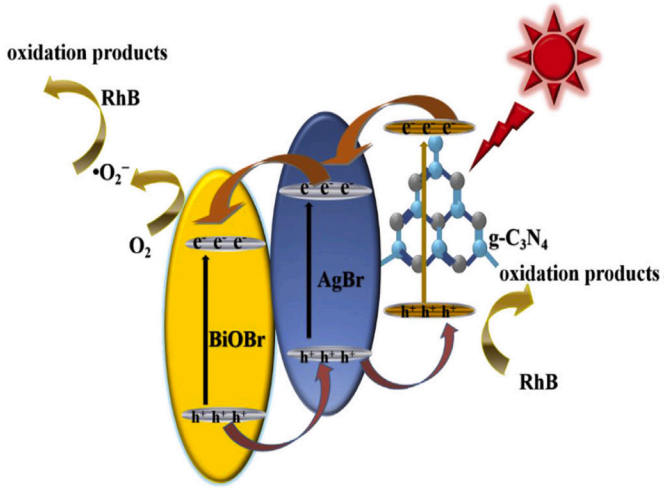

Fig. 4. Schematic illustration of possible visible-light-driven photocatalytic mechanism in ternary AgBr/g-C_3N_4/BiOBr system. (Reproduced with permission from Ref (Tang et al., 2019) Copyright Elsevier 2019).

ion exchange, then integrated with $NiFe_2O_4$ nanoparticles through a precipitation for magnetic separability. The BiOBr has a uniform flower-like morphology of self-assembled nanosheets, while both the AgBr and $NiFe_2O_4$ were nanoparticles of different sizes. These nanoparticles were well anchored on the petals of the flower-like BiOBr in the ternary composite. The AgBr functioned as a recombination mediator, while $NiFe_2O_4$ introduced magnetic functionality without hindering light absorption. Operating under visible light, the system displayed 100 % degradation of Rhodamine B within 90 min. The authors attributed this to a dual direct Z-scheme mechanism with one Z-scheme alignment between AgBr and BiOBr and another between BiOBr and $NiFe_2O_4$ (Fig. 5). This was inferred from the identification of superoxide radicals and holes as main oxidants through EPR analysis and quenching tests. Importantly, this catalyst was easily separated after use under a magnetic field, which is ideal for reusability and it retain 94 % of its efficiency after four cycles.

Pushing further toward real-world applicability, Cui et al. (2024) introduced a $BiOBr/ZnFe_2O_4$–GO ternary system synthesized via a one-pot hydrothermal method. This photocatalyst brought together the photothermal properties of graphene oxide (GO), the magnetic recovery of $ZnFe_2O_4$, and the oxidative potential of BiOBr. The composite achieved excellent tetracycline degradation under both visible and NIR light, and also allowed photothermal detection of pollutants. GO facilitated broad light absorption and acted as an electron highway, while the S-scheme configuration supported redox potential preservation. The work exemplifies how BiOBr-based systems can be tailored for synergistic catalysis beyond pollutant degradation. A similar integration of magnetic and catalytic functionality was also reported by Sabit and Ebrahim, who developed a $BiOBr/ZnFe_2O_4/CuO$ composite via co-precipitation and hydrothermal synthesis (Sabit and Ebrahim, 2023). The composite formed dual S-scheme heterojunction and promoted directional migration of photogenerated charge carriers which minimized recombination. The system demonstrated high efficiency in degrading malachite green dye, reaching over 98 % degradation within 60 min under LED light. Magnetic separability also enabled facile recovery and reuse for multiple cycles. Likewise, ternary $g\text{-}C_3N_4/BiOBr/Fe_3O_4$ has shown excellent magnetic functionality and improved photocatalytic performance (Preeyanghaa et al., 2022).

On the BiOI front, Wu et al. synthesized a ternary $GO/BiOI/NiWO_4$ heterojunction photocatalyst via a stepwise hydrothermal approach and investigated its performance through a combination of experimental techniques and density functional theory (DFT) simulations (Wu et al., 2024b). The integration of $NiWO_4$ facilitated efficient hole trapping due to its favorable band alignment, while GO enhanced electron transport and provided a high surface area for active site distribution. The optimized composite (10 wt% GO) exhibited exceptional photocatalytic activity, achieving up to 98.6 % degradation of methylene blue under visible light, with similarly high efficiency observed for rhodamine B. DFT and time-dependent DFT calculations revealed the formation of interfacial I–Bi–O–Ni(W) bonds and validated a Z-scheme charge transfer mechanism, which promotes efficient spatial separation of photogenerated electron–hole pairs and enhances the generation of reactive oxygen species. The GO-based architecture also contributed to increased light absorption and suppressed carrier recombination, underpinning the superior photocatalytic performance. This study confirmed the suitability of BiOI ternary heterostructured composite as efficient catalyst in wastewater treatment.

A more advanced system was introduced by Huang et al., who synthesized a double Z-type heterojunction comprising AgI, $Ag_6Si_2O_7$, and BiOI through ultrasonic-assisted co-precipitation and photoreduction techniques (Huang et al., 2024). This ternary composite, optimized at a 1/3 M ratio of AgI to $Ag_6Si_2O_7$ with 65 % BiOI by mass, demonstrated excellent photocatalytic efficiency, achieving 92.96 % degradation of norfloxacin (NOR) under visible light. Notably, the catalyst also significantly mitigated the toxicity of the treated effluent, as confirmed by wheat germination assays. The high performance was attributed to the formation of a double Z-scheme heterojunction, which facilitated spatial charge separation and efficient directional migration of photogenerated carriers as shown in Fig. 6. Within this architecture, Ag-based components serve multiple functions. AgI contributes to plasmonic sensitization, while both AgI and $Ag_6Si_2O_7$ act as electron mediators, enabling rapid interfacial charge transfer and minimizing recombination losses. Consequently, the system not only enhances visible light absorption but also promotes the generation of highly reactive species, thereby boosting both the photocatalytic activity and mineralization capacity. This work underscores the synergistic advantage of BiOI-based ternary Z-scheme configurations in optimizing redox potential alignment and reactive species generation for advanced water purification.

Altogether, these systems illustrate the flexibility of BiOX-based ternary heterostructures in addressing the limitations of pristine materials. The inclusion of CQDs, rGO, or GO dramatically boosts charge mobility and extends light absorption, while magnetic oxides provide practical separation. S-scheme and Z-scheme configurations, particularly those involving Ag-based or carbon-mediated interfaces, demonstrate strong redox performance and pollutant degradation, with many

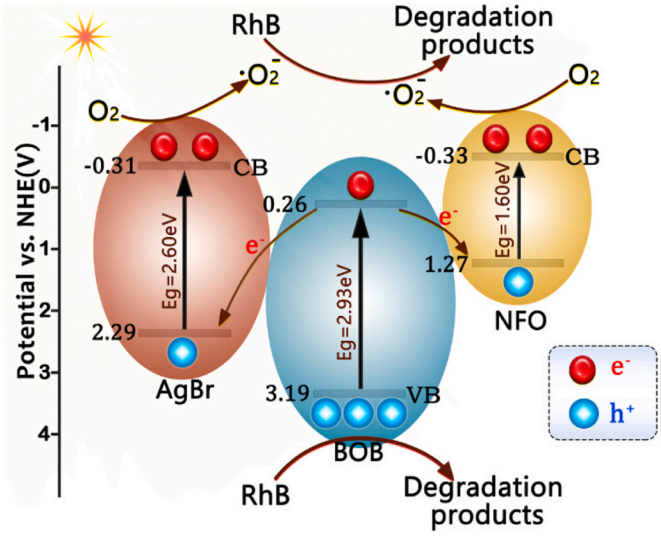

Fig. 5. Schematic diagram for $AgBr/BiOBr/NiFe_2O_4$ charge separation under visible light (Reproduced with permission from Ref (Jiang et al., 2022) Copyright Elsevier 2022).

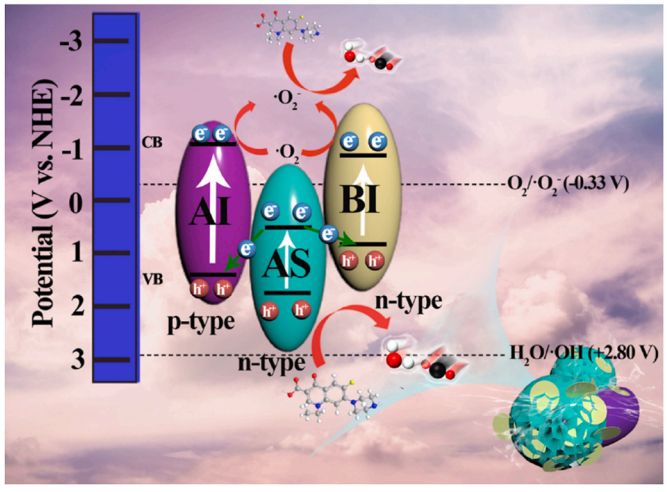

Fig. 6. Plausible electron transfer mechanism of photocatalytic removal of NOR by $AgI/Ag_6Si_2O_7/BiOI$ catalyst (Reproduced with permission from Ref (Huang et al., 2024) Copyright Elsevier 2024).

systems achieving more than 90 % removal within 60 min. The development of membrane-integrated or multifunctional hybrids further expands the relevance of these materials beyond laboratory-scale trials.

3.4. Bi_2MoO_6-based ternary heterojunctions

Bi_2MoO_6, a member of the Aurivillius family, has gained considerable attention as a visible-light-responsive photocatalyst owing to its

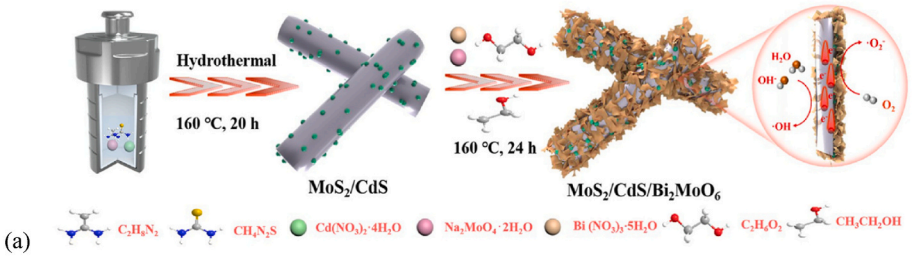

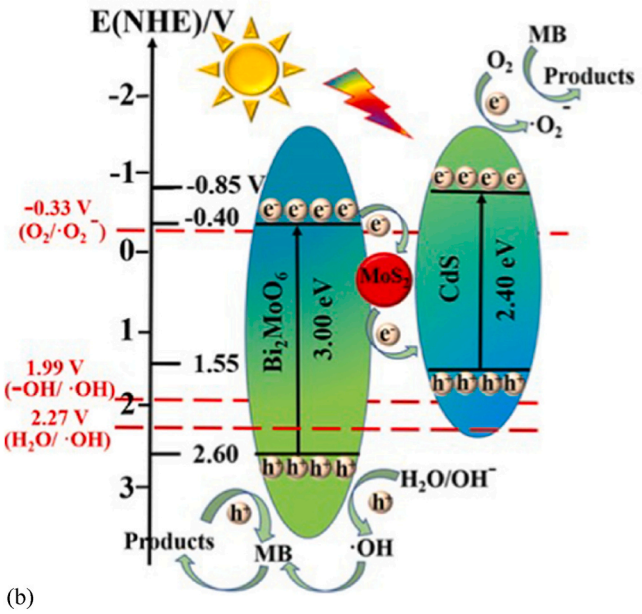

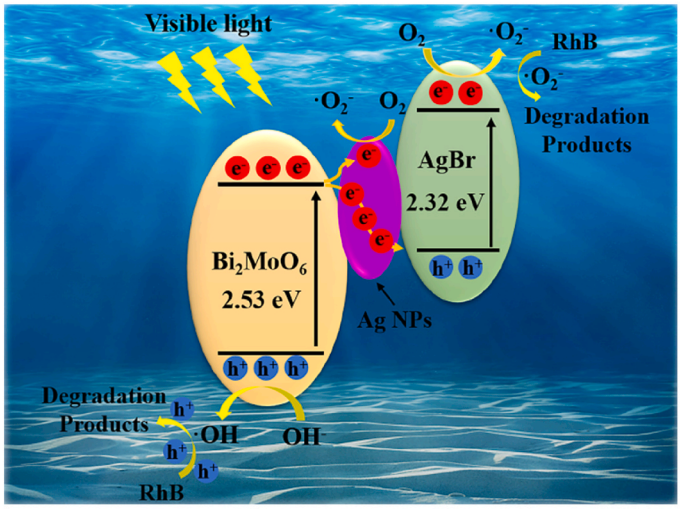

Fig. 7. (a) Schematic illustration of the fabrication process of Z-Scheme heterojunction $MoS_2/CdS/Bi_2MoO_6$ (b) The possible photocatalytic mechanism of Z-scheme $MoS_2/CdS/Bi_2MoO_6$ heterostructure for degradation of MB under visible light irradiation (Reproduced with permission from Ref (Z. Wang et al., 2023) Copyright Elsevier 2023) (c) The proposed mechanism for photo-degradation process of $Ag/AgBr/Bi_2MoO_6$ (Reproduced with permission from Ref (Cao et al., 2024) Copyright Elsevier 2024).

unique layered orthorhombic structure and narrow bandgap (~2.7 eV). Its high oxidative capability and structural stability make it a viable candidate for environmental remediation (Lin et al., 2023; G. Yin et al., 2022). However, the photocatalytic performance of pristine Bi_2MoO_6 is hampered by sluggish charge mobility and rapid recombination of photoinduced carriers. In recent years, substantial efforts have been made to construct Bi_2MoO_6-based ternary heterostructures, especially those incorporating 2D materials, noble metals, and semiconductor co-catalysts, to enhance charge separation and extend light absorption. The rational design of Z-scheme and S-scheme heterojunctions involving Bi_2MoO_6 enables preservation of strong redox abilities while facilitating interfacial charge transport.

A representative example is the ternary MoS_2/CdS/Bi_2MoO_6 photocatalyst reported by Wang et al., which was synthesized using stepwise hydrothermal and solvothermal treatments (Z. Wang et al., 2023). As shown in Fig. 7a, the MoS_2/CdS binary composite was first prepared through a hydrothermal route at 160 °C for 20 h before incorporating Bi_2MoO_6 microspheres via a second-step hydrothermal synthesis. The results showed that the MoS_2 nanoparticles and Bi_2MoO_6 microspheres were well anchored on the CdS, forming a ternary heterojunction. The photocurrent response of the MoS_2/CdS/Bi_2MoO_6 was twice that of the binary MoS_2/CdS, which revealed improved charge separation within the ternary composite. The intimate interface between MoS_2 and CdS created a direct Z-scheme pathway with Bi_2MoO_6, enabling efficient directional flow of electrons and holes (Fig. 7b). Consequently, the ternary photocatalyst achieved 96 % degradation of methylene blue and 73.5 % total organic carbon removal within 2 h under visible light, exhibiting high reusability over five cycles. The co-presence of MoS_2 contributed not only to extended light absorption but also acted as a reactive center for electron capture, enhancing charge transfer efficiency between CdS and Bi_2MoO_6. This study demonstrated the superiority of Bi_2MoO_6 based ternary systems to binary composites under visible light.

A similar structurally elegant approach was described by Gao et al., who constructed a dual Z-scheme g-C_3N_4/Bi_2MoO_6/CeO_2 heterojunction using a combination of solvothermal and calcination processes (Q. Gao et al., 2022). Bi_2MoO_6 was initially deposited on CeO_2 nanospheres, followed by g-C_3N_4 coating. The resulting composite facilitated multiple charge migration pathways, minimizing recombination and preserving oxidative radicals. A dual Z-scheme heterojunction was formed with one between Bi_2MoO_6 and CeO_2 and another between Bi_2MoO_6 and g-C_3N_4, which led to enhanced photocatalytic efficiency. The material achieved ~99 % degradation of 4-chlorophenol within 80 min under visible light. Radical scavenging studies showed the dominant role of hydroxyl radicals in the degradation pathway, supported by enhanced photoluminescence quenching and low charge transfer resistance.

MXene-mediated Bi_2MoO_6-based heterostructures are also very promising. For instance, Lin et al. constructed a Ti_3C_2-bridged Z-scheme Bi_2MoO_6-based photocatalyst, focusing on H_2 generation and norfloxacin removal (Lin et al., 2025). The catalyst was synthesized by facile solvothermal and subsequent thermal treatment, wherein Ti_3C_2 nanosheets provided a conductive platform between Bi_2MoO_6 and $ZnIn_2S_4$. The Bi_2MoO_6-$ZnIn_2S_4$/Ti_3C_2 composite exhibited superior norfloxacin degradation (96.49 % in 60 min) and high H_2 evolution activity, validating the dual function of MXene in both environmental and energy applications. Mechanistic analysis revealed that photogenerated electrons from Bi_2MoO_6 via the MXene recombine with the holes in the valence band of $ZnInS_4$, forming a Z-scheme heterojunction, and this effectively preserves the photogenerated holes in the Bi_2MoO_6 and the electrons in the conduction band of $ZnInS_4$, making them available for photocatalytic reactions, resulting in enhanced degradation of the Norfloxacin molecules. Similarly, Zhang et al. achieved improved mineralization of tetracycline using a PAN/Bi_2MoO_6/Ti_3C_2 composite (Zhang et al., 2022). The use of polyacrylonitrile (PAN) provided a flexible and porous membrane structure, while Ti_3C_2 offered excellent electrical conductivity and facilitated electron mobility. The MXene layers acted as bridges for electron flow in an S-scheme configuration, enabling effective migration from Bi_2MoO_6 to Ti_3C_2 and preventing electron–hole recombination. The ternary heterostructured achieved 97 % tetracycline degradation under visible light, with significant improvement in mechanical stability and photocatalytic reusability. Evidently, Mxene-modified Bi_2MoO_6-based ternary heterostructures possess remarkable photocatalytic efficiency.

Another approach is the incorporation of noble metals in Bi_2MoO_6 based composites. An example of this was reported by Wang et al., where a Pd/g-C_3N_4/Bi_2MoO_6 hollow microsphere composite was prepared via hydrothermal assembly and photoreduction (M. Wang et al., 2019). The Pd nanoparticles contributed an effective surface plasmon resonance effect, and Pd electrons, alongside the photogenerated electrons of the g-C_3N_4, were collected in the conduction band of Bi_2MoO_6, while the photogenerated holes from Bi_2MoO_6 transferred into the valence band of g-C_3N_4, forming a Type-II heterojunction mechanism. This efficient charge separation enhanced visible-light activity and resulted in 97 % degradation of rhodamine B within 40 min. The hollow structure also improved light scattering and reactant adsorption. Similarly, a Pt–$GdCrO_3$–Bi_2MoO_6 ternary heterojunction fabricated by hydrothermal and chemical precipitation methods has also shown high photocatalytic performance in both CO_2 reduction and water purification due to the formation of a Z-scheme heterojunction, underscoring the dual functional potential of Bi_2MoO_6-based systems (Jia et al., 2022). Additionally, Ag/AgBr/Bi_2MoO_6 ternary composite developed by Cao et al. (2024) through a straightforward hydrothermal and photoreduction techniques achieved 99.99 % removal of rhodamine B within just 12 min (Cao et al., 2024). The Ag served as an electron mediator in the Z-type heterojunction, promoting recombination of weak oxidative electrons from AgBr and weak reductive holes from Bi_2MoO_6, thereby preserving the strong redox potentials of the remaining carriers (Fig. 7c). The formation of superoxide and hydroxyl radicals, as verified by radical quenching and ESR analysis, confirmed that the Z-scheme mechanism effectively facilitated charge separation and prolonged carrier lifetimes. Hence, the addition of noble metals into Bi_2MoO_6-based composites offers a direct and fast approach in constructing Bi_2MoO_6 based ternary heterojunctions with high photocatalytic activity.

Moving beyond inorganic semiconductors and noble metals, Hu et al. introduced a natural clay-based composite, Bi_2MoO_6/g-C_3N_4/sepiolite, fabricated through ultrasonic dispersion and thermal treatment (Hu et al., 2023). Sepiolite, a fibrous clay mineral, offered a high surface area and acted as a structural support, while g-C_3N_4 served as a visible-light-active component. The ternary S-scheme heterojunction enabled selective degradation of tetracycline, with a reported degradation efficiency of ~93 % within 3 h. The mechanism was driven by efficient charge separation facilitated by internal electric fields between Bi_2MoO_6 and g-C_3N_4, with sepiolite aiding pollutant adsorption and catalytic stability. This work highlighted the role of structural supports in enhancing photocatalyst dispersibility and pollutant interaction.

These Bi_2MoO_6-based ternary heterostructures represent a diverse and promising class of photocatalysts for environmental remediation. Through rational design such as integrating conductive MXenes, porous clays, or noble metals, these composites succeed in addressing intrinsic limitations of Bi_2MoO_6. Most notably, the formation of S-scheme and dual Z-scheme junctions improves charge separation, suppresses recombination, and boosts redox reactivity. Many of these systems achieve pollutant degradation efficiencies exceeding 90 % within 60 min, while also offering structural stability and recyclability. These findings collectively underscore the versatility of Bi_2MoO_6 as a central component in advanced photocatalyst design and point toward future integration into multifunctional systems for simultaneous pollution abatement and resource recovery.

3.5. Bi_2S_3-based ternary heterojunctions

Bi_2S_3, a narrow-bandgap bismuth chalcogenide, has emerged as a promising component in ternary photocatalysts owing to its excellent light-harvesting ability, chemical stability, and low toxicity (Chawla et al., 2025; D et al., 2024). However, its photocatalytic activity when used alone is restricted by fast electron–hole recombination and limited surface area. To address these limitations, researchers have increasingly focused on constructing ternary heterostructures involving Bi_2S_3 to leverage synergetic charge transfer mechanisms, particularly through Z-scheme and S-scheme configurations. These approaches enable the retention of strong redox potentials while enhancing interfacial charge migration and improving structural stability under light irradiation.

One of the most structurally elegant systems is the $Bi_2S_3/MoS_2/TiO_2$ composite, reported by Drmosh et al. (2020). This photocatalyst was fabricated through microwave-assisted hydrothermal growth of Bi_2S_3 and MoS_2 on TiO_2 nanostructures, forming a spatially organized double Z-scheme configuration. In this setup, Bi_2S_3 and TiO_2 functioned as reduction and oxidation sites, respectively, while MoS_2 played the role of an electron mediator, enabling effective separation of the high-energy photogenerated carriers. The composite displayed excellent photocatalytic activity toward methylene blue degradation, attaining 99 % removal in less than 60 min under visible light. The Z-scheme mechanism retained strong oxidative and reductive species, enhancing both stability and efficiency. A similar Z-scheme strategy was employed by Wang et al. in their study of TiO_2 nanotubes/Bi_2S_3–MoS_2 composite (Q. Wang et al., 2023). This ternary structure was designed to couple photocatalytic pollutant degradation with hydrogen evolution. Bi_2S_3 and MoS_2 were sequentially deposited onto preformed TiO_2 nanotubes using hydrothermal methods, yielding a well-integrated 1D–2D–2D heterostructure. The material demonstrated dual functionality, achieving efficient degradation of organic dyes (73 % and 75.63 % removal of methyl orange and methylene blue, respectively, in 3 h) and sustaining H_2 production over multiple cycles. Time-resolved photoluminescence and photocurrent studies confirmed enhanced charge separation possibly driven by the spatial Z-scheme electron migration from Bi_2S_3 to MoS_2, while TiO_2 effectively captured and utilized photogenerated holes.

Expanding the synergy between Bi_2S_3 and MoS_2, Zhou et al. reported a fibrous $MoS_2/Bi_2S_3/BiFeO_3$ composite that demonstrated remarkable performance under piezo-photocatalytic conditions (Zhou et al., 2025). The material was prepared by electrospinning followed by hydrothermal synthesis, resulting in a fibrous morphology that enhanced mechanical coupling. Under ultrasonic vibration combined with visible-light irradiation, the ternary composite displayed a significantly improved degradation rate for rhodamine B, with over 94 % degradation within 50 min. The piezoelectric effect induced by $BiFeO_3$ assisted in separating photogenerated carriers, and the Z-scheme configuration with Bi_2S_3 and MoS_2 preserved oxidative radicals. This work revealed how external stimuli, such as mechanical energy, can synergize with band-engineered heterostructures to boost photocatalysis.

Ternary Bi_2S_3 systems have also shown promise in facilitating peroxymonosulfate (PMS)-mediated advanced oxidation processes. For example, in a study conducted by Sarkar et al., a dual Z-scheme g-C_3N_4/$ZnFe_2O_4/Bi_2S_3$ composite was constructed via microwave-assisted synthesis and optimized for the degradation of 2,4,6-trichlorophenol in the presence of PMS (Sarkar et al., 2022). The combination of Bi_2S_3 with magnetic $ZnFe_2O_4$ and visible-light-responsive g-C_3N_4 led to a multi-functional catalyst capable of degrading 98.9 % of the target pollutant within 40 min under visible light and PMS activation. The dual Z-scheme not only promoted directional charge migration but also facilitated electron–hole pair stabilization, as evidenced by scavenger experiments and radical quantification studies. The work highlighted the cooperative role of PMS in accelerating oxidative reactions and extending the function of Bi_2S_3 systems beyond conventional dye removal.

From a materials design standpoint, the integration of photothermal properties has also proven effective, as demonstrated by a study carried out by Jiang et al. on $Bi_2S_3/ZnS/g\text{-}C_3N_4$ ternary composite, where urchin-like Bi_2S_3 microspheres and ZnS quantum dots were co-deposited on mesoporous g-C_3N_4 nanosheets (Jiang et al., 2020). The system was synthesized through a stepwise solvothermal method and template-calcination process, optimizing both the light absorption and photothermal conversion properties. The resulting heterojunction demonstrated superior photothermal-photocatalytic performance, with approximately 99 % removal of Bisphenol An under simulated solar light. The mechanism involved a synergistic interaction between photogenerated carriers and localized heat, promoting faster reaction kinetics and broader spectral activation.

In another variation by also involving Bi_2S_3 and g-C_3N_4, Jabbar et al. reported a g-$C_3N_4/Ag_2WO_4/Bi_2S_3$ S-scheme heterojunction, prepared via ultrasonic mixing and in situ precipitation, targeting Congo red degradation in wastewater (Jabbar et al., 2023). The ternary composite showed improved visible light responsiveness, an indication of efficient charge separation, as observed in the photocurrent response measurement. The charge separation was facilitated through the formation of dual S-scheme heterojunction in the ternary composite due to the band alignment of the semiconductors. As shown in Fig. 8, the photogenerated electrons from Ag_2WO_4 are transferred and combined with the photogenerated holes in both the Bi_2S_3 and g-C_3N_4 making available well-separated photogenerated holes in the valence band of Ag_2WO_4 for the photocatalytic oxidation reaction. Consequently, the ternary catalyst achieved 98 % degradation of Congo red in 60 min under visible light, showing excellent recyclability and stability.

Certainly, Bi_2S_3-based ternary heterostructures have demonstrated impressive versatility across various configurations and environmental targets. Whether integrated with TiO_2, MoS_2, g-C_3N_4, ZnS, or $BiFeO_3$, the incorporation of Bi_2S_3 into Z- and S-scheme architectures significantly improves charge separation efficiency, pollutant mineralization rates, and light absorption breadth. These systems have consistently achieved over 90 % pollutant removal within short reaction periods and have shown good stability under repeated cycles. The adaptability of Bi_2S_3 across different structural morphologies, from spheres to nanotubes to fibers, and the possibility of combining photothermal, piezoelectric, and advanced oxidation effects positions Bi_2S_3 as a core component in next-generation photocatalytic strategies for wastewater purification.

3.6. Ternary heterojunctions with multiple bismuth-based compounds

Integrating multiple bismuth-based semiconductors into a single ternary heterojunction has emerged as a promising strategy to enhance visible-light-driven photocatalytic performance. Bismuth-containing compounds such as $BiVO_4$, BiOI, Bi_2MoO_6, Bi_2O_3, $BiFeO_3$, and BiOBr possess unique band structures, high photochemical stability, and strong visible light absorption. When two or more of these are intelligently combined, often alongside complementary materials such as g-C_3N_4, Ag_3PO_4, or SnS_2, they form heterojunctions that synergistically enhance charge separation, suppress recombination, and improve light harvesting. These multicomponent architectures, often arranged in Z-scheme, S-scheme, or n–n–p configurations, exploit the complementary properties of each constituent to boost photocatalytic degradation of organic pollutants, particularly antibiotics and dyes.

A notable demonstration of the power of combining multiple bismuth based compounds was reported by Zhou et al. who developed a $Bi_2MoO_6/g\text{-}C_3N_4/BiFeO_3$ ternary heterojunction (Zhou et al., 2022). Synthesized via sol-gel and solvothermal route, the photocatalyst showed significantly enhanced activity in the degradation of ciprofloxacin under visible light, with 95 % removal within 3 h. The inclusion of $BiFeO_3$ introduced a narrow-bandgap p-type component that established a p–n junction with Bi_2MoO_6, while g-C_3N_4 extended visible light response and facilitated electron migration. As shown in Fig. 9a, charge

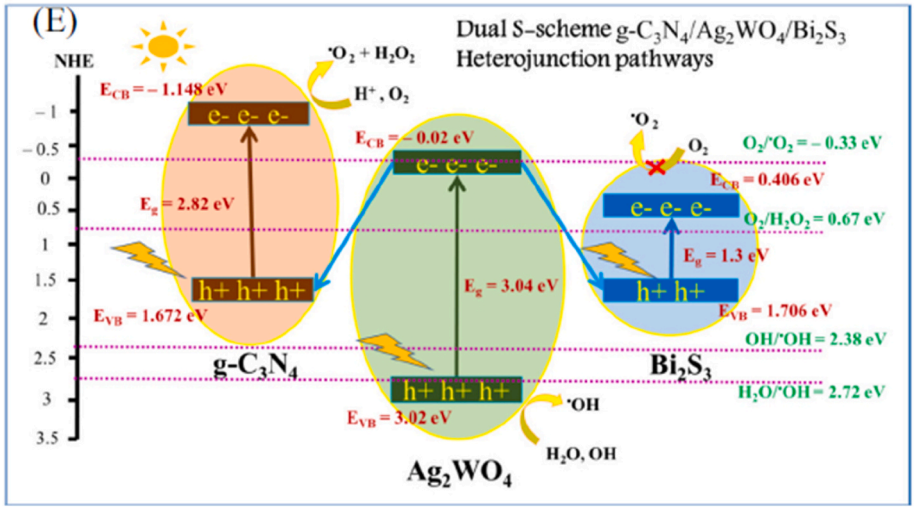

Fig. 8. Proposed dual S-scheme mechanism charge separation in g-C_3N_4/Ag_2WO_4/Bi_2S_3 (Reproduced with permission from Ref (Jabbar et al., 2023) Copyright Elsevier 2023).

separation was driven by a spatial Z-scheme heterojunction between g-C_3N_4 and $BiFeO_3$ while the photogenerated electrons in the conduction band of g-C_3N_4 also transferred into the conduction band of Bi_2MoO_6. Similarly trend was also observed in the ternary Bi_2MoO_6/-Bi_2O_3/Ag_3PO_4 (Sun et al., 2022). The composite exhibited superior degradation performance toward tetracycline with 77.4 % removal in 2 h. The inclusion of Bi_2O_3 and Bi_2MoO_6 promoted band alignment for directional electron flow, while Ag_3PO_4 served as a strong visible-light absorber and active redox center.

Utilizing two bismuth halides, Zheng et al. constructed of a BiOCl/BiOBr/SnS_2 composite, utilizing a double S-scheme charge transfer model (Zheng et al., 2024). The photocatalyst was synthesized through a stepwise solvothermal and chemical co-precipitation. The S-scheme configuration successfully separated the photo-induced carriers with SnS_2 acting as electron sink for both BiOCl and BiOBr photogenerated electrons, leading to a marked increase in visible-light photocatalytic activity. The photocatalyst achieved ~95 % degradation of rhodamine B dye in 20 min and the XRD analysis after four cycles showed that the photocatalyst structure remained unchanged while maintaining about 90 % degradation efficiency. Insights into the charge separation mechanism and the advantage of coupling two BiOX in a ternary heterojunction were provided through ESR analysis, ultraviolet photoelectron spectroscopy (UPS) and quenching experiments. It was noted that the energy band levels of BiOCl and BiOBr were well positioned relative to those of SnS_2 in such a way that when BiOCl, BiOBr and SnS_2 are in contact with each other, electrons flow from higher to lower Fermi levels, and holes do the opposite leading to negative charges accumulating on the BiOCl and BiOBr sides, and positive charges accumulate on the SnS_2 side. Simultaneously, an internal electric field is formed to bend the band, leading to the establishment of a new thermodynamic equilibrium leading to an efficient separation of charges within the SnS_2 semiconductor corresponding to S-scheme mechanism.

In a related work involving BiOX, Zhang et al. reported the preparation of $CuInS_2$/BiOI/Bi_2MoO_6 composite engineered to facilitate dechlorination of 2,4-dichlorophenol (Zhang et al., 2025). The ternary heterojunction was obtained through a solvothermal route, leading to a well-dispersed interface that promoted charge separation possibly through a Z-scheme mechanism. The material achieved ~80 % removal of 2,4-DCP and exhibited selective dechlorination ability, attributed to the charge migration from $CuInS_2$ to Bi_2MoO_6 while preserving oxidative holes in BiOI. The suitability of the catalyst towards the treatment real wastewater effluent was also assessed by studying the effect of humic acid on the degradation process and it was found that even though HA consumed part of the generated radicals, the degradation efficiency was still above 75 %. Also, the photocatalyst showed good stability over ten cycles and the XPS gross spectrum of the used photocatalyst did not detect any elemental residue. Hence, this catalyst has a good potential for wastewater treatment.

The integration of $BiVO_4$ with other bismuth based compounds in ternary heterostructures have also been investigated. For example, a ternary BiOI/$BiVO_4$/g-C_3N_4 composite with a dual Z-scheme heterojunction have been successful constructed and applied for the removal of different antibiotics (Zhu et al., 2022). The composite with a flower-globular structure was synthesized through successive hydrothermal and solvothermal processes. The morphology study revealed that $BiVO_4$ particles well distributed on the surface of g-C_3N_4 and BiOI which were in close contact. The ternary composite showed enhanced visible light absorption according to the reported UV–visible diffuse reflectance spectra. The BiOI/$BiVO_4$/g-C_3N_4 achieved remarkable degradation of levofloxacin, tetracycline, ceftriaxone sodium and oxytetracyline with highest removal of 89.1 % for leveofloxacin. These result exceeded the values obtained using pristine and binary composites of $BiVO_4$/g-C_3N_4. The improved performance was attributed to the possible formation of dual Z-scheme heterojunction in the ternary composite which preserved photogenerated electrons in BiOI and g-C_3N_4, while photogenerated holes were retained in the valence band of $BiVO_4$ (Fig. 9b) as supported with results from EPR and quenching experiments. This configuration proved effective in maintaining strong redox potentials while enhancing carrier lifetime. In earlier studies, it has been established that BiOI and $BiVO_4$ are excellent couple for heterojunction formation due to their band edge positions (Orimolade et al., 2019). Typically in such settings, the BiOI efficiently absorb visible light and $BiVO_4$ provide strong oxidative potential which complement the weak of oxidation ability of BiOI due to its relatively low valence band position. Hence, the addition of g-C_3N_4 further led to the formation of a more robust catalyst with better photocatalytic efficiency.

Building on this theme, Gao et al. (2022) introduced an S-scheme MoS_2/Bi_2S_3/$BiVO_4$ composite embedded within a 3D sponge (B. Gao et al., 2022b). The system, synthesized via solvothermal methods, was applied to the photo-Fenton degradation of fluoroquinolones. The synergistic interaction between MoS_2 and Bi_2S_3 enabled efficient visible-light absorption, while $BiVO_4$ supported hole migration. The catalyst demonstrated strong degradation kinetics and excellent cycling stability, with PMS activation further accelerating the breakdown of persistent pharmaceutical compounds. The utility of combining $BiVO_4$ with other bismuth oxides was further emphasized in the development

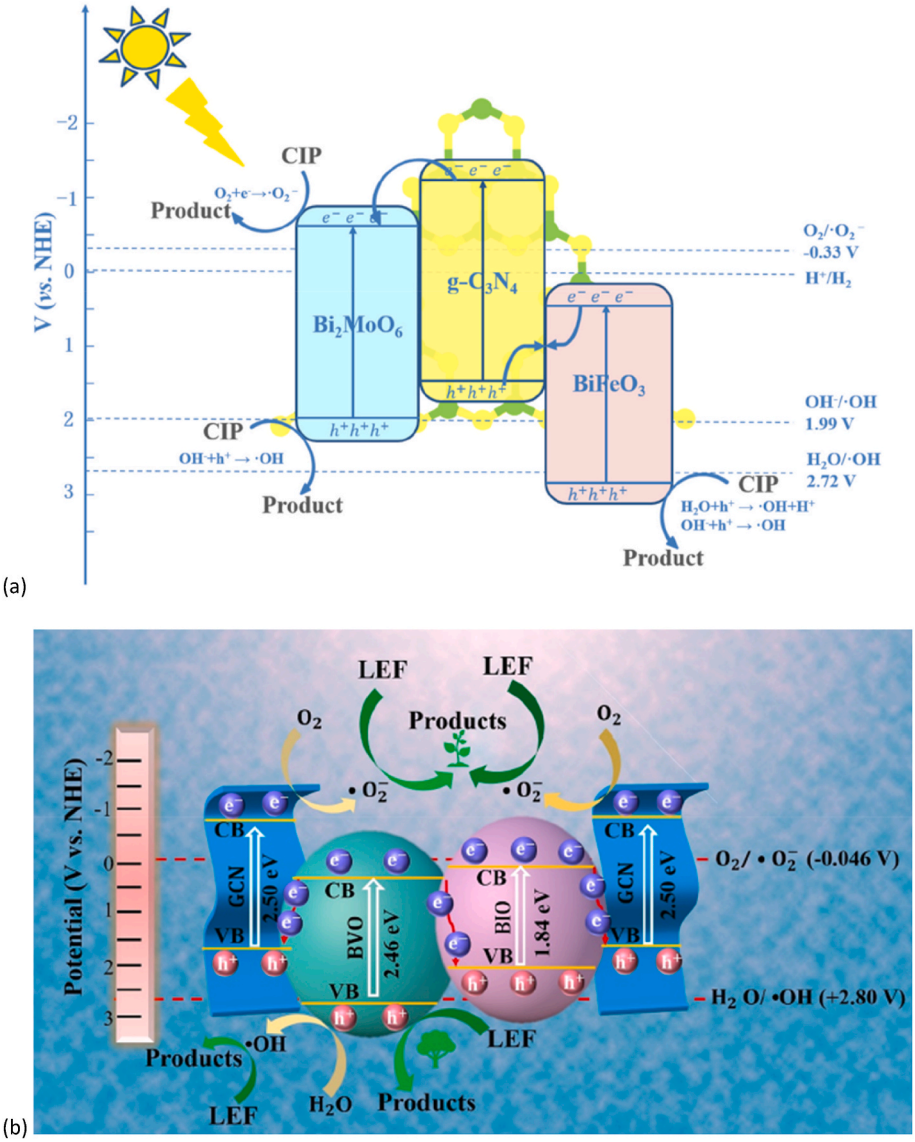

Fig. 9. (a) Proposed photocatalytic mechanism of $Bi_2MoO_6/g\text{-}C_3N_4/BiFeO_3$ (Reproduced with permission from Ref (Zhou et al., 2022) Copyright Elsevier 2022) (b) Plausible dual Z-scheme electron transfer mechanism in $BiOI/BiVO_4/g\text{-}C_3N_4$ (Reproduced with permission from Ref (Zhu et al., 2022) Copyright Elsevier 2022).

of a $BiVO_4/Bi_2WO_6/WO_3$ composite, which showed excellent degradation of dyes and antibiotics and was capable of inactivating *E. coli* (Cho et al., 2023). The spatial alignment of the band structures allowed for charge migration across the heterointerfaces, resulting in enhanced photodegradation rates and broad-spectrum antimicrobial action. When Bi_2WO_6 with intermediate band gap is coupled with $BiVO_4$ which has a more positive valence band, the resulting interface junction promotes the accumulation of photogenerated holes on $BiVO_4$ while WO_3 acts as electron sink for both $BiVO_4$ and Bi_2WO_6. The heterostructured photocatalyst demonstrated good stability over five cycles. Impressively, the toxicity assessment performed by incubation of 293T cells and zebrafish embryo composites confirmed great biocompatibility and low cytotoxicity of the photocatalyst.

For wide-spectrum pollutant degradation, ternary heterostructures containing entirely bismuth-based compounds have been fabricated. For example, Kumar et al. introduced a $BiPO_4/BiOBr/BiFeO_3$ composite, where Ag nanoparticles were photodeposited to enhance visible light response (Kumar et al., 2019a). The material achieved efficient degradation of norfloxacin under various light conditions, showing adaptability across UV, visible, and near-infrared regions. The multi-component structure promoted multichannel charge transport and radical generation, making it suitable for applications under fluctuating environmental illumination. In this system BiOBr enhances visible-light absorption through its internal dipole orientation and layered structure, which promotes rapid electron extraction and polar-driven charge separation. $BiPO_4$, with its wide bandgap and strong oxidizing valence band, supplies powerful photogenerated holes that drive deep oxidative mineralization of antibiotics under UV and visible light. $BiFeO_3$, a multiferroic semiconductor with intrinsic ferroelectric polarization, introduces an internal electric field that significantly aids directional charge movement across the heterojunction. The synergy between these components translated to improved photocatalytic efficiency. Likewise, Wang et al. developed a $Bi_4Ti_3O_{12}/Bi_2O_3/Bi_{12}TiO_{20}$ ternary system through a one-step sol-gel method (L. Wang et al., 2020). The spherical morphology enhanced light scattering and active surface area, while the internal Z-scheme configuration preserved oxidative potential. The photocatalyst demonstrated high degradation efficiency of methylene blue (100 % in 100 min) and was structurally stable across repeated uses, illustrating how multiple titanium-based bismuth phases can operate cooperatively.

In summary, these multicomponent systems showcase the potential of engineering ternary heterojunctions composed exclusively or

predominantly of bismuth-based semiconductors, with or without auxiliary materials. The carefully designed Z-scheme, S-scheme, and n–n–p heterostructures consistently demonstrate strong photocatalytic activity for the removal of dyes, pharmaceuticals, and bacteria, achieving degradation rates often exceeding 90 % under visible light. These configurations also enable extended light utilization, improved photostability, and application across varying environmental targets, reinforcing the versatility of bismuth-based ternary systems in modern photocatalytic applications.

3.7. Benchmarking of bismuth-based ternary heterostructured photocatalysts

A detailed evaluation of the photocatalytic performance of bismuth-based ternary heterostructured materials across recent literature reveals consistent advances in pollutant degradation efficiency, photogenerated charge separation, and structural engineering. According to the summary presented in Table 1, it is evident that bismuth based ternary heterostructures exhibit exceptional activity under visible light irradiation. This is attributed largely to the effective formation of charge separation pathways, tailored band edge potentials, and synergistic interfacial interactions among the three components.

Several bismuth-based ternary systems demonstrated complete pollutant removal under visible-light irradiation, with BiOBr playing a central role in enabling this high-level performance. Examples include BiOBr/g-C_3N_4/CQDs and g-C_3N_4/BiOBr/Fe_3O_4, which achieved 100 % removal of tetracycline within 60 min. The layered structure of BiOBr provides intrinsic anisotropic charge transport arising from its internal electric field generated by the $[Bi_2O_2]^{2+}$ slabs and halide layers. In both systems, the dominant contribution of BiOBr, through its polarization-induced internal field, broad visible-light absorption, and high-valence-band oxidation strength, underpins the full mineralization performance and demonstrates its utility as a potent central component in high-efficiency ternary heterostructures. Beyond BiOBr-based systems, complete pollutant removal has also been achieved in ternary architectures centered on $BiVO_4$, most notably the TiO_{2-x}/$Bi_4V_2O_{11}$/$BiVO_4$ composite. In this heterostructure, $BiVO_4$ acted as the primary visible-light harvester owing to its narrow band gap and electronic structure dominated by the V-3d/O-2p hybridized valence band, which provided strong photoactivity under solar wavelengths. Its intrinsically high valence-band position endowed the system with powerful oxidative capability, enabling rapid generation of reactive oxygen species. When coupled with oxygen-deficient TiO_{2-x}, which supplied abundant surface defects and broad-spectrum absorption, $BiVO_4$ benefitted from accelerated electron extraction into defect-rich TiO_{2-x} domains. The addition of $Bi_4V_2O_{11}$ formed a complementary conduction pathway due to its mixed ionic-electronic conductivity and flexible layered structure, which supports multidirectional charge migration. Likewise, almost complete degradation of organic pollutant was observed with the use $BiVO_4$/rGO/$FeVO_4$ and Co_3O_4-$BiVO_4$/g-C_3N_4 ternary heterostructures.

Ternary systems such as g-C_3N_4/BiOBr/Fe_3O_4 and BiOBr/$ZnFe_2O_4$-GO not only achieved above 90 % removal of tetracycline within 50–60 min, but also integrated additional functionalities such as magnetic separability and photothermal synergism. These features not only support higher degradation efficiency but also offer practical advantages in catalyst recovery and continuous operation, both of which are critical for real-world wastewater treatment systems. The observed rate constants in these composites were consistent with rapid kinetics, with values in the range of 0.033–0.040 min^{-1}. Furthermore, their performance remained stable after multiple reuse cycles, indicating good structural robustness and photochemical stability.

Photocatalysts such as Bi_2MoO_6/g-C_3N_4/sepiolite demonstrated outstanding photocatalytic performance in the degradation of tetracycline, achieving 97.2 % removal within 60 min and an apparent rate constant (k) of 0.7108 min^{-1} under visible light. This high activity stems from the S-scheme configuration supported by sepiolite's layered morphology, which provides both a high surface area and a network for directional charge migration. Similarly, the ternary BiOBr/$ZnFe_2O_4$/CuO composite displayed robust degradation of malachite green dye, reaching 96.9 % removal and a rate constant of 0.0397 min^{-1}. The enhanced performance in this system was attributed to dual S-scheme electron transfer and strong magnetic separation capability, which favored reusability without activity loss.

A notable observation from the benchmarking table is the increasing reliance on S-scheme and dual Z-scheme mechanisms in achieving efficient pollutant removal. These charge transfer modes, as observed in systems like Ag@$BiPO_4$/BiOBr/$BiFeO_3$ and $BiVO_4$/Bi_2WO_6/WO_3, enable the retention of high redox potential by preserving the photogenerated electrons in the conduction band of one semiconductor and holes in the valence band of another, thereby promoting simultaneous oxidation and reduction reactions. In the case of $BiVO_4$@$ZnIn_2S_4$/$Bi_2Sn_2O_7$, a dual Z-scheme heterojunction structure contributed to 97.3 % removal of tetracycline in 60 min, with the mechanism aided by optimal band matching and visible-light absorption enhancement across the composite interface.

Carbon-based frameworks, especially g-C_3N_4 and graphene oxide, were frequently employed as electron mediators or support materials to promote interfacial contact and inhibit recombination. For example, the incorporation of CQDs into the BiOBr/g-C_3N_4 system significantly elevated the rate of tetracycline degradation to 98.1 % within 60 min. This result can be attributed to the role of CQDs as a conductive bridge facilitating the rapid transfer of electrons, as well as their contribution to visible light absorption. Likewise, GO-modified heterojunctions such as GO/BiOI/$NiWO_4$ and GO/$Bi_2O_2CO_3$/$NiWO_4$ demonstrated high tetracycline and malachite green removal with extended activity into the near-infrared range, benefitting from enhanced photothermal conversion and expanded light utilization.

Several of the composites also exploited the use of bimetallic oxides and sulfides in combination with bismuth phases to tailor redox selectivity. For instance, the BiOCl-Cu_2CoSnS_4-TiO_2 system utilized the electronic properties of Cu and Co sulfides to facilitate visible-light activity and direct Z-scheme transfer. This structure achieved 93.1 % degradation of direct blue dye within 60 min, underscoring the benefits of band structure engineering in fine-tuning charge mobility. Similarly, systems based on BiOI and layered oxides, such as AgI/$Ag_6Si_2O_7$/BiOI, produced synergistic effects through heterojunction refinement and showed accelerated removal of antibiotics within 45 min.

Dual or successive Z-scheme systems, such as CdS/Bi_2MoO_6/BiOBr and BiOI/$BiVO_4$/g-C_3N_4, further demonstrated how introducing an additional charge mediator or stepwise band offset could drive more efficient spatial separation and faster surface reactions. These systems typically reported degradation efficiencies above 95 % within 1 h, with consistent kinetic profiles and retention of catalytic performance over multiple runs. Interestingly, some composites extended functionality beyond photocatalysis into photo-Fenton processes or electrocatalytic activity. For example, the Fe_3O_4@CeO_2@BiOI system exhibited dual capability for PMS activation and UVA-driven degradation, offering versatility in advanced oxidation process frameworks. Its fast pollutant removal (94.4 % in 40 min) further attested to the cooperative role of redox-active metals and bismuth oxides in enhancing degradation rates.

A meaningful cross-comparison of photocatalytic performance remains inherently challenging because the apparent rate constant alone does not fully capture the influence of operational parameters. As shown across the dataset, experimental conditions such as catalyst dosage, pollutant concentration, solution volume, pH, background ionic strength, reactor geometry, and most critically irradiance vary widely between studies, yet many papers do not report these parameters in sufficient detail. This inconsistency complicates direct benchmarking because the degradation kinetics of any photocatalytic system are strongly dependent on photon availability rather than catalyst characteristics alone. Ideally, performance should be normalised using photon flux or quantum efficiency metrics (AQY or EQE), but most studies did

Table 1
Recent studies of bismuth-based ternary heterojunctions in removal of pollutants.

Photocatalysts	Heterojunction	Photocatalysis condition	%removal	K (min^{-1})	Ref
$AgBr/GO/Bi_2WO_6$	Z-Scheme	20 mg/L TC, 100 mL, 40 mg catalyst, 300W Xe lamp	84 % in 60 min	0.0515	Guan et al. (2021)
$TCPP/GO/Bi_2WO_6$	Z-scheme	15 mg/L TC, 100 mL, 30 mg catalyst, 300W Xe lamp	79.2 % in 60 min	–	Hu et al. (2019)
$GO/TiO_2/Bi_2WO_6$	Type II	Ethylene, 2 L, 50 mg catalyst, 500 W Xe lamp	–	0.0013	Xie et al. (2021)
$Au@TiO_2/Bi_2WO_6$	Z-scheme	15 mg/L TC/SMX, 100 mL, 50 mg catalyst, 300 W Xe lamp	96.9 % (SMX), 95 % (TC) in 75 min	0.0425 (SMX) 0.0314 (TC)	Jin et al. (2022)
$TiO_2/g\text{-}C_3N_4/Bi_2WO_6$	Type-II	10 mg/L BG, 100 mL, 15.76 mg catalyst, 300 W Xe lamp	99.72 % in 70 min	–	Mirhosseini et al. (2022)
$BiVO_4@ZnIn_2S_4/Bi_2Sn_2O_7$	Dual Z-scheme	5 mg/L RhB, 30 mL, 10 mg catalyst, 300 W Xe lamp	81 % in 60 min	0.027	Zhang et al. (2021)
$AgI/ZnIn_2S_4/BiVO_4$	Dual Z-scheme	20 mg/L TC, 50 mL, 30 mg catalyst, 300 W Xe lamp	91.44 % in 150 min	0.02112	S. Wang et al. (2022)
$BiVO_4/rGO/FeVO_4$	Z-scheme	0.15 g/L MB, 100 mL, 0.1 g catalyst, 300 W Xe lamp	99.52 % in 120 min	–	Alomayri (2025)
$Co_3O_4\text{-}BiVO_4/g\text{-}C_3N_4$	Z-scheme	80 mg/L KN-R, 50 mL, 30 mg catalyst, 300 W Xe lamp	99.6 % in 30 min	0.5018	(Yile Wang et al., 2020)
$Ag_2CO_3/Bi_4O_5I_2/g\text{-}C_3N_4$	Dual S-scheme	20 mg/L TC, 50 mL, 30 mg catalyst, 300 W Xe lamp	82.16 % in 30 min	0.0389	Chen et al. (2022)
$Ag_2CO_3/BiOBr/WO_3\text{-}x$	Dual Z-Scheme	2 x 10^{-5} M MB, 100 mL, 50 mg catalyst, 300 W Xe lamp	97 % in 60 min	0.0210	Sharma et al. (2024)
$BiOBr/CdTe/TiO_2$	Type-II	10 mg/L MO, 50 mL, 100 mg catalyst, 500 W Xe lamp	75 % in 120 min	0.0082	Qu et al. (2019)
$BiOBr/g\text{-}C_3N_4/CQDs$	Z-scheme	10 mg/L TC, 40 mL, 40 mg catalyst, 500 W Xe lamp	100 % in 60 min	0.0922	Chen et al. (2024)
$BiOCl\text{-}Cu_2CoSnS_4\text{-}TiO_2$	Type-II	20 mg/L DB71, 80 mL, 100 mg catalyst, 300 W Xe lamp	91.48 % in 60 min	0.0270	Chowdhury et al. (2022)
$BiOI/CuInS_2/ZnO$	Dual S-scheme	10 mg/L TC, 100 mL, 60 mg catalyst, 500 W Xe lamp	96.75 % in 90 min	0.0324	Banyal et al. (2024)
$CDs@BiOI/g\text{-}C_3N_4$	Z-scheme	20 mg/L TC, 100 mL, 30 mg catalyst, 30 W LED	82.7 % in 60 min	0.0290	C. Yin et al. (2022)
$Cs/MnO_2/BiOCl$	Z-scheme	10 mg/L MB, 100 mL, 10 mg catalyst, 300 W Xe lamp	98 % in 40 min	0.0810	Hong et al. (2022)
$Fe_3O_4@CeO_2@BiOI$	Type-II	10 mg/L SMX, 50 mL, 10 mg catalyst, UVA	97 % in 15 min	0.2210	Kohantorabi et al. (2021)
$g\text{-}C_3N_4/BiOBr/Fe_3O_4$	Z-scheme	15 mg/L TC, 40 mL, 20 mg catalyst, 300 W Halogen lamp	100 % in 60 min	–	Preeyanghaa et al. (2022)
$Li\text{-}C_3N_4/ZnO/BiOI$	Type-II and Z-scheme	10 mg/L TC, 100 mL, 50 mg catalyst, 200 W Xe lamp	92.62 % in 30 min	–	Jiang et al. (2024)
$NCQDs\text{-}BiOBr\text{-}TiO_2/PVDF$	Type-II	10 mg/L TC, 20 mL, 10 mg catalyst, 300 W Xe lamp	77 min in 120 min	0.0134	Luo et al. (2021)
$NH_2\text{-}UiO\text{-}66/BiOBr/AgI$	Dual Z-scheme	10 mg/L TC, 50 mL, 20 mg catalyst, 300 W Xe lamp	97 % in 40 min	–	Qiu et al. (2023)
SnO_2–BiOBr–rGO	Type-II	20 mg/L MB, 50 mL, 20 mg catalyst, 300 W Xe lamp	99.8 % in 90 min	–	Dhillon et al. (2024)
$ZnO@BiOBr/UiO\text{-}66\text{-}NH_2$	Dual Z-scheme	20 mg/L TC, 50 mL, 0.4 g/L catalyst, LED lamp	98.2 % in 90 min		Ghorbani et al. (2023)
$MoS_2/CdS/Bi_2MoO_6$	Z-scheme	10 mg/L MB, 50 mL, 30 mg catalyst, 300 W Xe lamp	96 % in 2 h	0.0256	Z. Wang et al. (2023)
$Bi_2MoO_6/ZnIn_2S_4/Ti_3C_2$	Z-scheme	31.21 mg/L NOR, 50 mL, 0.47 g/L catalyst, 300 W Xe lamp	96.49 % in 60 min	0.07	Lin et al. (2025)
$Bi_2MoO_6/g\text{-}C_3N_4/sepiolite$	S-scheme	40 mg/L TC, 50 mL, 50 mg catalyst, 500 W Xe lamp	92.7 % in 3 h	0.7108	Hu et al. (2023)
$Bi_2O_3/Biochar/g\text{-}C_3N_4$	Z-scheme	20 mg/L TC, 50 mL, 1 g/L catalyst, 500 W Xe lamp	86.7 % in 30 min	0.0610	Huang et al. (2023)
$Bi_2O_3/BN/Co_3O_4$	Type-I	5 mg/L NOR, 50 mL, 50 mg catalyst, 500 W Xe lamp	98 % in 3 h	–	Wang et al. (2024)
$Bi_2O_3/CuBi_2O_4/Ag$	S-scheme	10 mg/L EE2, 100 mL, 40 mg catalyst, 250 W Xe lamp	94.6 % in	0.0185	Majhi et al. (2021)
Bi_2O_3–$CuBi_2O_4$–CuO	Dual Z-scheme	10 mg/L MB, 100 mL, 100 mg catalyst, 300 W Xe lamp	100 % in 70 min	0.0332	Hou et al. (2022)
$Fe_2O_3/Bi_2O_3/TiO_2$	Dual S-scheme	50 mg/L SMZ, 100 mL, 20 mg catalyst, 300 W Xe lamp	98 % in in 60 min	–	Algarni et al. (2024)
$MoO_3/Bi_2O_3/g\text{-}C_3N_4$	Z-scheme	10 mg/L TC, 50 mL, 50 mg catalyst, 500 W Xe lamp	98 % in 140 min	–	Alnaggar et al. (2021)
$TiO_2/MgBi_2O_6/Bi_2O_3$	n-n-p junction	10 mg/L TC, 50 mL, 100 mg catalyst, 50 W LED lamp	99.5 % in 90 min	–	Pournemati et al. (2022)
$Ag/g\text{-}C_3N_4/Bi_3TaO_7$	Z-scheme	5 mg/L SMZ, 50 mL, 25 mg catalyst, 300 W Xe lamp	98 % in 25 min	0.1499	Ren et al. (2019)
$Ag\text{-}Bi_{12}GeO_{20}\text{-}Bi_2WO_6$	Type-II	10 mg/L RhB, 50 mL, 30 mg catalyst, 300 W Xe lamp	99 % in 16 min	0.452	Lv et al. (2019)
$AgBr/Bi_4Ti_3O_{12}/Bi_2Sn_2O_7$	S-scheme	30 mg/L RhB, 30 mL, 30 mg catalyst, 300 W Xe lamp	100 % in 2 h	0.0059	N. Li et al. (2024)
$Bi_2O_2CO_3/Bi_2O_2(OH)NO_3/g\text{-}C_3N_4$	Type-II	20 mg/L RhB, 50 mL, 100 mg catalyst, 300 W Xe lamp	94.3 % in 60 min	0.0476	Wu et al. (2020)

(*continued on next page*)

Table 1 (*continued*)

Photocatalysts	Heterojunction	Photocatalysis condition	%removal	K (min^{-1})	Ref
$Bi_3O_4Br/Bi_2O_2CO_3/g\text{-}C_3N_5$	Dual Z-scheme	20 mg/L RhB, 50 mL, 15 mg catalyst, 450 W gold halide lamp	90 % in 2 h	0.0200	W. Wang et al. (2025)
$CdS/Bi_2MoO_6/BiOBr$	Z-scheme	30 mg/L TC, 50 mL, 50 mg catalyst, 65 W Xe lamp	94.41 %	0.0605	R. Wang et al. (2021)
$BiOI/AgI/Bi_2WO_6$	Dual S-scheme	20 mg/L TC, 30 mL, 30 mg catalyst, 300 W Xe lamp	94 % in 60 min	0.109	H. Luo et al. (2023)
$Bi_{12}O_{17}Cl_2/Sb_2O_3$/MWCNT	Type-I	20 mg/L CBZ, 100 mL, 30 mg catalyst, 150 W LED lamp	90.2 % in 75 min	0.0129	Jabbar et al. (2025)
$MoS_2/g\text{-}C_3N_4/Bi_{24}O_{31}Cl_{10}$	Dual Z-scheme	20 mg/L TC, 50 mL, 100 mg catalyst, 300 W Xe lamp	97.5 % in 50 min	0.0643	Kang et al. (2020)
$g\text{-}C_3N_4/BiVO_4\text{-}Bi_2WO_6$	Type-II	20 mg/L RhB, 40 mL, 40 mg catalyst, 300 W Xe lamp	96.7 % in 60 min	0.058	Hu et al. (2021)
$Fe_3O_4/BiOCl/BiOI$	Z-scheme	40 mg/L TC, 50 mL, 20 mg catalyst, 300 W Xe lamp	89 % in 80 min	0.0193	Dang et al. (2022)
$g\text{-}C_3N_4$@Au@$Bi_4Ti_3O_{12}$	Type-II	5 mg/L RhB, 200 mL, 20 mg catalyst, 200 W Xe lamp	94.4 % in 60 min	0.0238	Gao et al. (2020)
$GO/Bi_2O_2CO_3/NiWO_4$	Z-scheme	40 mg/L MB, 100 mL, 30 mg catalyst, 300 W Xe lamp	99.34 % in 60 min	–	Wu et al. (2024a)
TiO_2-QDs/BiOBr/BiOCl	Type-II	10 mg/L RhB, 30 mL, 100 mg catalyst, 50 W LED lamp	98.8 % in 15 min	0.2346	Shoja et al. (2020)
$TiO_{2\text{-}x}/Bi_4V_2O_{11}/BiVO_4$	Dual S-scheme	6.2×10^{-5} TC, 200 mL, 0.15 g catalyst, 50 W LED lamp	100 % in 2 h	0.020	Saadati et al. (2023)
$WO_3/BiVO_4/BiOCl$	Type-II	10 mg/L RhB, 50 mL, 25 mg catalyst, 300 W Xe lamp	75 % in 2 h	–	Li et al. (2019)
$ZnO–ZnBi_2O_4$/RGO	Z-scheme	80 mg/L MB, 100 mL, 40 mg catalyst, 570 W Xe lamp	100 % in 4 h	–	Hosseinzadeh et al. (2022)
$\alpha\text{-}Bi_2O_3/\beta\text{-}Bi_2O_3/Bi_5O_7I$	Dual S-scheme	20 mg/L BPA, 50 mL, 50 mg catalyst, 500 W Xe lamp	80.4 % in 5 h	0.0462	Kan et al. (2023)

not provide the necessary information such as the incident photon flux (einstein.L^{-1}.min^{-1}), spectral distribution, or cutoff wavelengths. Consequently, photon-normalised comparisons could only be attempted for a limited number of reports where light intensity/irradiance (mW.cm^{-2}) was clearly stated.

For these representative cases as shown in Table 2, the apparent rate constant (k) was divided by the irradiance to yield a normalised rate constant (k_{norm}) expressed in $cm^2.mW^{-1}.min^{-1}$, providing a more equitable basis for comparison. Although the number of studies reporting irradiance was small, the results reveal clear differences in the intrinsic activity of various ternary heterostructures. Systems such as $Pd/g\text{-}C_3N_4/Bi_2MoO_6$ and $\alpha\text{-}Bi_2O_3/\beta\text{-}Bi_2O_3/Bi_5O_7I$ exhibited the highest k_{norm} values (0.00585 and 0.00462 cm^2 $mW^{-1}.min^{-1}$, respectively), indicating efficient utilization of incident photons. Their superior performance aligns with the presence of strong internal electric fields and plausible S or Z scheme charge transfer channels. In comparison, materials such as $MoS_2/CdS/Bi_2MoO_6$ and $g\text{-}C_3N_4/Ag_2WO_4/Bi_2S_3$ showed lower k_{norm} values despite high removal efficiencies, suggesting substantial dependence on high photon input rather than intrinsically faster charge separation. These results emphasize that degradation percentages alone may mask fundamental differences in photocatalytic efficiency when light intensity is not accounted for.

Overall, the benchmarking results confirm that bismuth-based ternary heterojunctions have evolved into a highly adaptable platform for environmental remediation. The average pollutant removal across the reported systems is consistently above 90 %, and most materials achieve this within 30–90 min under visible light, demonstrating a strong alignment with practical operation conditions. The highest-performing systems tend to integrate multiple synergistic elements: engineered band alignment, extended visible-light absorption, conductive support frameworks, magnetic or recoverable features, and optimized morphology.

Going forward, further improvements in activity, selectivity, and stability will depend on advancing material design to include stronger interface bonding, incorporation of light-scattering or plasmonic elements, and deployment of green synthesis protocols. Moreover, while

Table 2
Recent studies of bismuth-based ternary heterojunctions in removal of pollutants with normalised rate constants.

Photocatalysts	Heterojunction	Reaction condition	%removal	K (min^{-1})	K_{norm} ($cm^2.mW^{-1}.min^{-1}$)	Ref
$MoS_2/CdS/Bi_2MoO_6$	Z-scheme	10 mg/L MB, 50 mL, 30 mg catalyst, 300 W Xe lamp, 100 mW/cm^2	96 % in 2 h	0.0256	0.000256	Z. Wang et al. (2023)
$Bi_2O_3–CuBi_2O_4–CuO$	Dual Z-scheme	10 mg/L MB, 100 mL, 100 mg catalyst, 300 W Xe lamp; 80 mW/cm^2	100 % in 70 min	0.0332	0.000415	Hou et al. (2022)
$\alpha\text{-}Bi_2O_3/\beta\text{-}Bi_2O_3/Bi_5O_7I$	Dual S-scheme	20 mg/L BPA, 50 mL, 50 mg catalyst, 500 W Xe lamp, 10 mW/cm^2	80.4 % in 5 h	0.0462	0.00462	Kan et al. (2023)
$Pd/g\text{-}C_3N_4/Bi_2MoO_6$	Type II	10 mg/L RhB, 50 mL, 10 mg catalyst, 300 W Xe lamp; 16 mW/cm^2	97 % in 40 min	0.0936	0.00585	M. Wang et al. (2019)
MIL-53(Fe)/$\alpha\text{-}Bi_2O_3/g\text{-}C_3N_4$	Z-scheme	10 mg/L amido black, 50 mL, 20 mg catalyst, 35 W Xe lamp; 67 mW/cm^{-2}	100 % in 45 min	0.0834	0.00124	Cui et al. (2020)
NH2-MIL-101(Fe)@MCN/Bi_2O_3	S-scheme	10 mg/L TC, 50 mL, 20 mg catalyst, 300 W Xe lamp; 180 mW/cm^2	100 % in 50 min	0.0294	0.000163	Li et al. (2023)
$g\text{-}C_3N_4/Ag_2WO_4/Bi_2S_3$	S-scheme	20 mg/L Congo Red, 250 mL, 50 mg catalyst, 300 W Xe lamp, 111 mW/cm^2	98 % in 60 min	0.0543	0.000489	Jabbar et al. (2023)
$AgI/Ag_6Si_2O_7/BiOI$	Dual Z-scheme	20 mg/L NOR, 50 mL, 30 mg catalyst, 65 W lamp, 60 mW/cm^2	92.96 % in 2 h	0.01241	0.000207	Huang et al. (2024)
$BiOBr/ZnFe_2O_4/CuO$	Dual S-scheme	25 mg/L MG, 250 mL, 150 mg catalyst, 150 W LED lamp, 120 mW/cm^2	98 % in 90 min	0.03483	0.000290	Sabit and Ebrahim (2023)

kinetic metrics such as apparent rate constants provide useful benchmarks, the limited availability of irradiance data underscores the need for stricter reporting standards in photocatalysis research. Normalised metrics such as AQY, EQE, and k_{norm} should be routinely included in future studies to enable fair comparison across materials and to assess whether observed improvements arise from genuine advances in heterostructure design or merely from differences in illumination conditions. The present analysis demonstrates the value of normalisation but also highlights the constraints imposed by incomplete experimental reporting across the literature. Additionally, comprehensive testing in real wastewater matrices, long-term cycling studies, and toxicity profiling of degradation intermediates remain critical steps in validating these materials for industrial application. The diversity and adaptability demonstrated in the current performance landscape clearly highlight the potential of bismuth-based ternary heterojunctions as a cornerstone in next-generation photocatalytic wastewater treatment technologies.

3.8. Energy band structures and charge transfer mechanisms in bismuth-based ternary heterostructures

A central determinant of the photocatalytic efficiency of bismuth-based ternary heterostructures is the nature of their energy band alignment and the resulting charge-transfer pathway. Since these systems rely strongly on different interfacial configurations, their band structure ultimately governs the separation, lifetime, and redox ability of photogenerated carriers. In majority of bismuth-based ternary heterostructures, Type II, Z-scheme and S-scheme heterojunctions are commonly proposed as the charge-transfer mechanisms. However, in many studies, the plausible mechanism determined through quenching experiment in photocatalysis and PL measurements were not fully confirmed using other reliable analysis such as the in-situ XPS or DFT calculations.

In classical type-II heterojunctions, the staggered band structure enables spatial electron–hole separation whereby electrons migrate from the semiconductor with a higher CB to the one with a lower CB while holes migrate in the reverse direction. The plausible mechanism in systems such as g-C_3N_4/BiOBr/AgBr (Tang et al., 2019), TiO_2/Bi_2WO_6/g-C_3N_4 (Mirhosseini et al., 2022) and NCQDs/BiOBr/TiO_2 (Luo et al., 2021; Luo et al., 2021) conform to this behavior. This mechanism is highly reliable but sacrifices redox strength because the accumulated electrons and holes lie in energetically weaker positions. As a result, type-II structures often fail to mineralize recalcitrant pollutants without assistance.

To preserve strong oxidative and reductive potentials, many bismuth-based ternaries adopt Z-scheme heterojunctions, in which the mechanism resembles natural photosynthesis. In a Z-scheme, the photogenerated electron in the lower-energy CB recombines with the photogenerated hole in the higher-energy VB of a second semiconductor. This leaves behind a strongly reducing electron in a high-energy CB (typically in $ZnIn_2S_4$, CdS, or WO_3) and a strongly oxidizing hole in a deep VB (typically in $BiVO_4$, Bi_2MoO_6, or Bi_2WO_6). Evidence for Z-scheme behavior is widely documented across the dataset, including in systems such as Bi_2WO_6/WO_3/$BiVO_4$ (Cho et al., 2023), AgI/$ZnIn_2S_4$/-$BiVO_4$ (S. Wang et al., 2022), CdS/Bi_2MoO_6/BiOBr (R. Wang et al., 2021), and MoS_2/CdS/Bi_2MoO_6 (Z. Wang et al., 2023). These materials consistently show enhanced radical generation, high photocurrent responses, and suppressed PL, all of which suggest effective Z-scheme charge transfer. In the case of Bi_2O_3/Bi/$ZnIn_2S_4$, the charge separation mechanism was further confirmed through first-principles density functional theory (DFT) calculations which revealed that Bi nanoparticles were sandwiched between Bi_2O_3 and $ZnIn_2S_4$ acting as a mediator (J. Luo et al., 2023). Also, the charge density difference map revealed pronounced electron accumulation and depletion at the interface region indicating strong electron coupling and hybridization among the components which makes Z-scheme mechanism possible.

The more recently conceptualized S-scheme heterojunction is mechanistically distinct from the Z-scheme, although both preserve strong redox capability. Unlike Z-scheme structures, which involve the recombination of photogenerated carriers between two semiconductors, the S-scheme relies on internal electric-field-driven recombination within a band-bending region created upon Fermi-level alignment. In an S-scheme, the semiconductor with a higher Fermi level becomes an n-type component with upward band bending, while the lower-Fermi-level semiconductor becomes p-type or quasi-p-type with downward bending. The resulting built-in field selectively recombines “weak” carriers (low-energy electrons and holes) while retaining the “strong” electrons in the reduction photocatalyst and the “strong” holes in the oxidation photocatalyst (F. Li et al., 2024). This mechanism is supported by UPS and XPS band-offset measurements, ESR radical generation patterns, and I–V rectification in systems such as Bi_2MoO_6/g-C_3N_4/sepiolite (Hu et al., 2023), BiOBr/$ZnFe_2O_4$/CuO (Sabit and Ebrahim, 2023), g-C_3N_4/BiOBr/Fe_3O_4 (Preeyanghaa et al., 2022), and MoS_2/-Bi_2S_3/$BiVO_4$ (B. Gao et al., 2022b). Importantly, the S-scheme explains why these composites maintain strong oxidative holes in Bi_2MoO_6 or $BiVO_4$ while simultaneously supporting highly reducing electrons in g-C_3N_4, $ZnFe_2O_4$, or MoS_2.

Accurate classification of charge transfer in heterojunctions is central to rational photocatalyst design because the photocatalytic outcome depends on which carriers are retained and which recombine at the interface. Two mechanisms that are often conflated in the literature are the Z-scheme and the S-scheme. Both permit strong redox potentials to be retained compared with Type-II junctions, but they differ fundamentally in the origin of selective recombination, the nature of the mediator (if any), the role of built-in fields, and the experimental signatures that validate them Z-scheme systems rely on physical recombination between two semiconductors either directly or via an electron mediator enabling the retention of the most reactive carriers but requiring sufficiently intimate interfacial contact for recombination (Li et al., 2022). In contrast, S-scheme systems rely on internal band bending that forms a unidirectional built-in electric field, where selective recombination occurs only within the depletion region (F. Li et al., 2024). While Z-scheme junctions are driven by energetic differences between bands, S-scheme junctions are driven primarily by Fermi-level equilibration and internal electrostatic fields. Thus, Z-scheme photocatalysts emphasize redox preservation through deliberate recombination, whereas S-scheme photocatalysts emphasize directional carrier migration through strong internal fields (Zulfa et al., 2024). Both mechanisms appear widely in bismuth-based ternaries, but S-scheme structures often demonstrate better charge-separation efficiency because their built-in field reduces recombination loss and enhances electron mobility.

Beyond Z-scheme and S-scheme systems, some bismuth-based ternaries incorporate p–n or p–n–n junctions, such as BiOCl/BiOBr/SnS_2 (Zheng et al., 2024) or $CuInS_2$/BiOI/Bi_2MoO_6 (Zhang et al., 2025). These heterojunctions create extended depletion regions and strong internal fields that promote accelerated interfacial charge transfer, supported by Mott–Schottky plots and EIS data. Some systems further employ conductor-mediated pathways such as rGO in $BiVO_4$/rGO/-$FeVO_4$ (Alomayri, 2025) or Ag in Ag@$BiPO_4$/BiOBr/$BiFeO_3$ (Kumar et al., 2019b) which provide high-mobility electronic bridges.

Evidently, the remarkable photocatalytic performance of bismuth-based ternary heterostructures arises not from the addition of a third component alone, but from engineered energy-band configurations that tailor charge flow, interfacial electric fields, and redox capability. By integrating S-scheme, Z-scheme, type-II, p–n, and conductor-mediated charge-transfer strategies, these materials consistently overcome the intrinsic recombination limitations of single semiconductors, enabling superior degradation of antibiotics, dyes, phenolics, and emerging pollutants across the reviewed systems.

3.9. Morphology-driven assembly of ternary bismuth heterostructures

The photocatalytic performance of ternary bismuth-based heterostructures is governed not only by their band structures and interfacial charge transfer but also by the morphological frameworks through which these interfaces are constructed. Morphology determines surface area, defect density, crystallite orientation, facet exposure, reactant accessibility, and the spatial distribution of heterojunction interfaces (Zhou et al., 2023, 2024a). Consequently, the development of ternary composites has increasingly shifted toward morphology-engineered architectures that simultaneously optimize light absorption, carrier mobility, and catalytic robustness. Across the literature, several recurring structural frameworks emerge, including hierarchical microspheres, two-dimensional layered frameworks, one-dimensional nanorod or nanofiber-mediated assemblies, core–shell constructs, hollow and porous structures, and surface-decoration or anchored nanospecies. Each strategy bears distinct advantages for photocatalysis while also introducing material-specific weaknesses that influence stability, synthetic feasibility, and scalability.

Hierarchical microsphere and flower-like assemblies are frequently employed because they combine high surface area with abundant defect-rich junctions. In many ternary systems such as Co_3O_4/$BiVO_4$/g-C_3N_4 (Yile Wang et al., 2020), WO_3/$BiVO_4$/BiOCl (Li et al., 2019) and AgBr/BiOBr/$NiFe_2O_4$ (Jiang et al., 2022), the interwoven flake or petal-like subunits provide exposed active facets and shortened diffusion pathways for photocarriers. Their radial architecture allows reactants to diffuse readily toward inner reaction chambers which reduces mass-transfer problems. However, these complex morphologies often depend on hydrothermal conditions that require careful templating or surfactant control. Small changes in pH, precursor concentration, or aging time can result in morphological collapse or inconsistent formation of tertiary interfaces. Moreover, the thermal and mechanical stability of flower-like assemblies sometimes remains limited, particularly under long-term irradiation, where structural disorder may increase recombination rates.

Two-dimensional (2D) nanosheet–nanosheet heterostructures represent another widely adopted approach. A typical example is the BiOBr/g-C_3N_4/Carbon quantum dots heterostructured which was prepared through electrostatic self-assembly method (Chen et al., 2024). The ultrathin layers in 2D frameworks often create intimate face-to-face contact, which is highly beneficial for constructing extended interfacial regions capable of fast charge separation. Also, the planar geometry maximizes lateral conductivity and promotes directional electron flow. Furthermore, such 2D frameworks provide tunable surface terminations and easier integration with the third component which could be metallic nanoparticles, quantum dots, or secondary semiconductor (Fu et al., 2021; M. Wang et al., 2019). Their primary weakness lies in their tendency to restack due to van der Waals attractions. This can restrict light harvesting and obstruct the creation of well-dispersed ternary junctions unless additional spacers, surface modifiers, or exfoliation steps are introduced, which in turn complicate synthesis and may introduce impurities.

One-dimensional architectures such as nanorods, nanobelts, and electrospun fibers offer a different set of advantages by promoting anisotropic charge transport. When materials such as Bi_2S_3, $BiVO_4$, or TiO_2 nanotubes serve as the backbone of a ternary system, the elongated pathways direct charge carriers along preferential axes, reducing interfacial scattering (Drmosh et al., 2020; Q. Wang et al., 2023). Electrospun fibers, in particular, provide mechanically robust platforms for loading additional components without severe aggregation, enabling continuous-flow applications (Zhang et al., 2022). Despite these benefits, the integration of multiple components onto 1D structures frequently requires precise control of nucleation kinetics. Nonuniform deposition or uneven surface anchoring can cause partial coverage, hindering the intended charge transfer paths. Moreover, excessive deposition of the third component can overly block active sites or inhibit light penetration, reducing apparent activity (Zhou et al., 2025).

Core–shell and yolk–shell morphologies allow even more deliberate spatial separation of carrier pathways. When a bismuth oxide or bismuth oxyhalide core is encapsulated within a shell of a second semiconductor and decorated with a third functionality (such as noble metal, magnetic phase, or co-catalyst), the geometry promotes directional, radial charge migration. Such architectures exhibit strong structural confinement, limiting agglomeration and providing excellent recycling stability (Ghorbani et al., 2023; Huang et al., 2024; Qu et al., 2019). However, synthesizing well-defined core–shell–shell or hollow ternary frameworks often demands multi-step procedures, prolonged calcination, or template removal methods. These increase synthetic cost and may introduce residues that interfere with photocatalytic reactions (Chen et al., 2024; Dhillon et al., 2024). Additionally, mismatched thermal expansion between layers can lead to microcracks during irradiation or recycling.

Hollow, mesoporous, and hierarchically porous architectures which are frequently reported in Bi_2MoO_6, BiOI, and Bi_2WO_6 based ternary composites play a pivotal role in enhancing photocatalytic performance by providing expansive internal surface area and multiple light-scattering pathways that prolong photon residence time. For instance, 3D porous spherical TiO_2–Bi_2WO_6/GO frameworks exhibit intensified multiple scattering and improved diffusion of pollutants into the internal cavity regions, thereby facilitating more effective interfacial contact within the ternary junctions (Xie et al., 2021). Similarly, MIL-100(Fe) @Bi_2WO_6/g-C_3N_4 harnesses the intrinsic porosity of MOF-derived matrices to enable high pollutant accessibility and abundant reactive sites (Peyrovi et al., 2025), while porous rGO/Bi_2WO_6/TCPP networks exploit interconnected nanosheet channels to enhance light management and accelerate charge migration across interfaces (Hu et al., 2019). Hollow microspherical $Bi_4Ti_3O_{12}$/Bi_2O_3/$Bi_{12}TiO_{20}$ structures further demonstrate the benefits of interior voids, which reduce bulk diffusion distances and promote radial charge separation (L. Wang et al., 2020). Despite these advantages, structural uniformity in hollow systems remains challenging, as cavity collapse or partial shell distortion can occur during high-temperature calcination, while lattice mismatch between components may compromise wall integrity. Moreover, highly porous architectures, although beneficial for adsorption and infiltration, may suffer from reduced local electronic density near heterointerfaces, potentially weakening the built-in electric fields required for directional charge transfer in S-scheme and Z-scheme photocatalysts. These limitations underscore the need for controlled templating, precise thermal processing, and careful interface tuning to fully capitalize on the morphological advantages of hollow and porous ternary bismuth systems.

Surface-anchored nanoparticles and quantum dots have become powerful tools for tuning reaction kinetics in ternary bismuth-based heterostructures, providing additional channels for charge extraction and extended visible-light absorption. Systems incorporating Ag or AgBr based nanoclusters, such as Ag/AgBr/Bi_2MoO_6 (Cao et al., 2024), AgI/$ZnIn_2S_4$/$BiVO_4$ (S. Wang et al., 2022), and AgI/$Ag_6Si_2O_7$/BiOI (Huang et al., 2024), demonstrate how plasmonic or Schottky-active noble metal domains can intensify local electromagnetic fields and facilitate rapid electron trapping. Likewise, carbon quantum dot–modified architectures like the CQDs/BiOBr/TiO_2 (Luo et al., 2021) and CQDs/BiOBr/g-C_3N_4 (Chen et al., 2024) heterostructures highlight the capacity of quantum-sized mediators to shuttle electrons across interfaces with minimal recombination losses. While these nanoparticle-anchored systems offer significant functional tunability, their practical deployment is hindered by stability concerns: migration or dissolution of Ag-based nanoparticles under irradiation, excessive surface loading that blocks active sites, or the gradual detachment of QDs and noble metal species during repeated cycling. Such degradation not only disrupts the integrity of the engineered heterojunction but also raises concerns regarding secondary contamination and increased operational cost, especially in continuous-flow or industrial water

treatment settings.

Altogether, morphological control in ternary bismuth-based photocatalysts is a decisive factor that dictates not only intrinsic charge dynamics but also practical deployment potential. Optimizing morphology requires balancing the advantages of hierarchical complexity, facet exposure, and interfacial density with the demands of structural robustness, reproducibility, and scalable synthesis. Future efforts should combine in situ characterization with predictive modeling to establish direct correlations between morphology, internal electric fields, and real-world photocatalytic durability. Such insights will be essential to develop morphologically engineered ternary systems that transcend laboratory success and achieve genuine applicability in wastewater treatment technologies.

3.10. Environmental safety, secondary pollution risks, and ecotoxicological considerations of bismuth-based ternary photocatalysts

Despite the growing sophistication and efficiency of bismuth-based ternary heterostructures, their environmental safety profile remains insufficiently discussed in the literature, and concerns surrounding potential secondary pollution require explicit consideration. Ternary photocatalysts incorporating Bi^{3+}, oxyhalides (BiOCl, BiOBr, BiOI), and sulfide-containing components (Bi_2S_3, $NiFe_2O_4$, $ZnFe_2O_4$, MoS_2, $CuInS_2$, SnS_2) introduce the possibility of ion leaching, dissolution of unstable phases, and release of nanosized fragments during repeated photocatalytic cycles (Han et al., 2025). Several studies acknowledge this risk indirectly through stability testing, yet very few quantify metal or halide release under operational conditions. For instance, systems such as $BiOBr/ZnFe_2O_4/CuO$ (Sabit and Ebrahim, 2023), $Fe_3O_4@CeO_2@BiOI$ (Kohantorabi et al., 2021), and $MoS_2/Bi_2S_3/BiVO_4$ (Gao et al., 2022) demonstrate good recyclability, but their reports do not include leachate analysis, leaving uncertainty regarding long-term environmental compatibility. Bi_2S_3 containing composites such as $Bi_2S_3/MoS_2/TiO_2$ (Drmosh et al., 2020) and $g\text{-}C_3N_4/ZnFe_2O_4/Bi_2S_3$ (Sarkar et al., 2022) may release sulfide species under acidic or oxidative conditions, while $CuInS_2/BiOI/Bi_2MoO_6$ (Zhang et al., 2025) and $BiOCl/BiOBr/SnS_2$ (Zheng et al., 2024) may similarly undergo partial halide or metal dissolution. These pathways underscore the importance of incorporating systematic leaching assessments into future studies, particularly when sulfides or halides constitute integral components of the heterostructures.

In few studies, however, where efforts were made to investigate the ecotoxicology impact of bismuth-based ternary heterostructures, the results are impressive. For instance, the toxicity analysis of $CuWO_4/Bi_2WO_6/MnS$ nanoparticles which was done using ECOSAR software revealed that the degraded products are non-toxic and the material can be safely utilized for environmental analysis. Also, the genotoxicity study which was done using *allium cepa* confirmed that there are no causes of cytotoxicity and genotoxicity by the prepared ternary heterostructured photocatalyst (Subhiksha et al., 2022). Similarly, $Bi/Bi_2S_3/Bi_2WO_6$ showed no sign of toxicity when its degradation solution was tested against rice seedlings (Ding et al., 2023). Furthermore, the $CdS/Bi_{20}TiO_{32}/Bi_4Ti_3O_{12}$ showed more than 90 % cell viability up to a concentration of 500 mgL^{-1} suggesting its non-cytotoxic nature and the results from atomic absorption spectroscopy revealed no leached ion from the photocatalyst into the solution (Das et al., 2022).

Beyond catalyst stability, the toxicity of degradation intermediates remains largely underexplored. Many pollutants treated in the reviewed literature including fluoroquinolone antibiotics, tetracycline, parachlorophenol, and nitrite or phenolic contaminants undergo multi-step oxidative transformation. However, few studies perform LC–MS identification of by-products, leaving the environmental fate of these intermediates uncertain. The generation of more toxic or recalcitrant species remains a plausible risk, particularly for halogenated antibiotics, azo dyes, and chlorophenols. Only a limited number of studies such as the toxicity elimination analyses in $Fe_3O_4@CeO_2@BiOI$ (Kohantorabi et al., 2021) and the antimicrobial assessments in $GO\text{-}In_2O_3/BiVO_4$ (Athar and Muneer, 2024) evaluate post-treatment toxicity, and even these do not provide ecotoxicity data across relevant trophic levels. The lack of information on chronic toxicity, biodegradability, and interaction of intermediates with aquatic organisms represents a significant knowledge gap, particularly for antibiotics whose reactive intermediates can disrupt microbial communities at low concentrations.

The potential ecotoxicity of spent photocatalysts also warrants focused attention. Ternary systems containing magnetic cores such as $NiFe_2O_4$ (Jiang et al., 2022), Fe_3O_4 (Preeyanghaa et al., 2022), or $ZnFe_2O_4$ (Sarkar et al., 2022) offer facile recovery but may still shed nanoscale debris after repeated cycling, potentially affecting benthic or filter-feeding organisms. Materials containing noble metals ($Ag/AgBr/Bi_2MoO_6$, $AgI/ZnIn_2S_4/BiVO_4$, $Ag@BiPO_4/BiOBr/BiFeO_3$) raise additional concerns given the known antimicrobial activity of silver ions and nano-Ag species. Likewise, photocatalysts incorporating carbon dots or graphene derivatives may introduce carbonaceous nanofragments whose long-term ecological effects remain poorly understood. Although recyclability assessments typically demonstrate >80–90 % retention of activity after several cycles, the environmental safety of recovered or discarded materials remains largely uncharacterized.

To align photocatalyst development with actual environmental management needs, future research on bismuth-based ternary heterostructures must integrate comprehensive ecotoxicological evaluations. This includes quantifying leached ions (Bi^{3+}, halides, sulfides, Co^{2+}, Fe^{3+}), identifying transformation by-products with LC–MS and GC–MS, evaluating acute and chronic toxicity using representative aquatic models (e.g., algae, Daphnia, fish embryos), and assessing the biodegradability and persistence of intermediates. Incorporating such safety assessments will not only strengthen the environmental relevance of bismuth-based photocatalytic systems but also support their future translation into real wastewater treatment settings.

3.11. Scalability and green chemistry considerations in ternary bismuth photocatalysts

Although significant progress has been made in designing high-performance bismuth-based ternary heterostructures, the scalability and industrial feasibility of their synthesis routes remain largely unaddressed in current research. Most of the reported fabrication strategies including hydrothermal/solvothermal synthesis, sol–gel processes, electrospinning, precipitation, and template-assisted self-assembly have been optimized for laboratory-scale production, with limited assessment of energy demand, solvent compatibility, reagent cost, or environmental footprint. Given that many of the ternary systems reviewed in this manuscript rely on multi-step or multi-solvent synthesis, a systematic evaluation of their scalability is essential for enabling real-world implementation.

Hydrothermal and solvothermal routes are the most frequently used methods in the reviewed literature because they offer excellent control over crystallinity, defect concentration, and heterointerface formation. Their sealed reaction environment enables the incorporation of multiple phases which favored the construction of ternary heterostructures like $BiOBr/Fe_3O_4/g\text{-}C_3N_4$ (Preeyanghaa et al., 2022), $BiVO_4/Ag/CdS$ (B. Gao et al., 2022a), and $FeO_4@CeO_2@BiOI$ (Gao et al., 2022; Kohantorabi et al., 2021) with well-defined junctions that are critical for Z-scheme or S-scheme behavior. However, hydrothermal synthesis suffers limitations when evaluated from a scalability perspective. It requires high pressure, prolonged heating (6–24 h), and often energy-intensive temperature control. For instance, the preparation of $Fe_3O_4/BiOCl/BiOI$ took 12 h at a temperature of 160 °C (Dang et al., 2022) while reaction time of 12 h at 180 °C was required for $BiOI/BiVO_4/g\text{-}C_3N_4$ (Zhu et al., 2022). Additionally, large-volume autoclaves for industrial scale production are costly, difficult to operate continuously, and pose safety concerns. Moreover, many reported systems rely on organic solvents such as

ethylene glycol, DMF, ethanol–water mixtures, which introduce hazards related to toxicity and solvent disposal. While hydrothermal synthesis is ideal for fundamental material design, its industrial adoption will require transitioning toward continuous-flow hydrothermal reactors or solvent-minimized processes.

Sol–gel–based synthesis offers better scalability than hydrothermal methods because it is conducted at ambient or moderately elevated temperatures, uses easily accessible precursors, and is suitable for large-batch production. For instance, ternary systems such as AgI/$Ag_6Si_2O_7$/BiOI (Huang et al., 2024), ZnO@BiOBr/UiO-66-NH_2 (Ghorbani et al., 2023), and TiO_2/Bi_2WO_6/g-C_3N_4 (Mirhosseini et al., 2022) benefit from the sol–gel route due to its uniform mixing and molecular-scale control. Nevertheless, sol–gel synthesis often relies on alcohols, chelating agents, and metal alkoxides that increase cost and present hazards during large-scale processing. Gelation and drying stages may also introduce cracking or inhomogeneity when the batch size increases. Optimizing sol–gel methods for industrial application therefore requires solvent recovery systems, low-toxicity precursors, and drying approaches that minimize shrinkage, such as supercritical drying or freeze-drying, although these also increase costs.

Electrospinning has emerged as a promising technique for constructing one-dimensional ternary heterostructures, especially $BiVO_4$ and Bi_2S_3 based nanofibers that benefit from directional charge transport and large surface area. Systems such as Bi_2MoO_6/Ti_3C_2 MXene membranes (Zhang et al., 2022), Bi_2O_3/$Bi_4Ti_3O_{12}$/$Bi_{12}TiO_{20}$ (L. Wang et al., 2020), and MoS_2/Bi_2S_3/$BiFeO_3$ (Zhou et al., 2025) illustrate the capability of electrospinning to produce flexible, immobilized photocatalysts suitable for wastewater filtration modules. Electrospinning is inherently scalable through multi-needle or needleless configurations, yet the need for polymeric carriers (such as PAN, PVP, PVDF), high-voltage equipment, and post-calcination steps increases energy consumption and complicates green chemistry metrics. Additionally, the use of solvent systems including DMF, acetone, NMP further raise toxicity and environmental concerns. Thus, while electrospinning holds significant industrial potential due to its ability to produce binder-free and easily recoverable composites, greener solvent systems and lower-temperature stabilization strategies must be advanced for effective adoption of this process.

Increasing attention is also directed toward the green chemistry attributes of bismuth-based ternary heterostructures, particularly as environmental applications require materials that are not only efficient but also sustainable and low-risk (Lu et al., 2022; Zhou et al., 2024b). A limited number of studies demonstrate early progress toward greener fabrication and operation. For example, employed bio-derived polymeric matrices such as PVA and starch films have been employed for immobilization Bi_2WO_6-based composites, reducing nanoparticle dispersion into solution and eliminating the need for harsh chemical binders (Li et al., 2021; Xie et al., 2022). Membrane-based systems such as the PVDF/CdS/Bi_2WO_6/ZnO hybrid (H. Wang et al., 2020) and the NCQD/BiOBr/TiO_2 photocatalytic membrane (Luo et al., 2021) further advance green design by providing reusable, immobilized architectures capable of continuous-flow operation, while carbon quantum dots used in the latter can be synthesized from biomass or low-cost organic waste. Another important route toward sustainability is magnetic recoverability, exemplified by AgBr/BiOBr/$NiFe_2O_4$ (Jiang et al., 2022), BiOBr/$ZnFe_2O_4$/CuO (Sabit and Ebrahim, 2023), and BiOBr/$ZnFe_2O_4$–GO (Cui et al., 2024), each of which significantly minimizes secondary pollution by enabling rapid and loss-free separation of photocatalysts after treatment. These emerging examples highlight that green chemistry principles are increasingly integrated into bismuth-based ternary photocatalysts, but their systematic adoption remains limited and warrants greater emphasis in future research.

For industrial translation, future research must rigorously evaluate solvent toxicity, waste generation, reaction yield, atom economy, and energy consumption. In addition, continuous-flow processing, spray-drying, flame aerosol synthesis, microwave-assisted methods, and solvent-free mechanochemical synthesis represent promising alternatives for scaling up bismuth-based ternary photocatalysts while meeting environmental and economic constraints. The integration of lifecycle assessment (LCA) and techno-economic analysis (TEA) into photocatalyst design will be essential to ensure that high photocatalytic performance is achieved without compromising environmental sustainability or economic feasibility.

4. Conclusion, recommendation and future perspectives

Bismuth based ternary heterostructured photocatalysts continue to demonstrate significant promise for visible light driven purification of contaminated water systems. Their performance advantage arises from the synergistic integration of multiple semiconductors that generate strong internal electric fields, promote spatially separated charge migration and maintain the high oxidative and reductive potentials needed to mineralize persistent pollutants. Across the wide range of materials reviewed, including Bi_2WO_6, $BiVO_4$, BiOX, Bi_2MoO_6, Bi_2S_3 and Bi_2O_3, ternary configurations consistently outperform their single component and binary counterparts. This is largely due to their enhanced interfacial contact, expanded optical absorption and strengthened intrinsic charge separation, which collectively underpin the high degradation efficiencies observed for dyes, pharmaceuticals, antibiotics, phenolic pollutants and recalcitrant organic species under visible and solar irradiation.

A clear conclusion from the literature is that the design concept for ternary heterostructures has progressed from conventional band matching toward more sophisticated interfacial architectures capable of regulating directional electron flow. Architectures such as S-scheme, Z-scheme, dual Z-scheme and n-n-p junctions promote targeted charge retention and efficient radical generation by controlling the spatial distribution of electrons and holes. Morphological engineering further contributes to photocatalytic performance. Hollow and mesoporous structures extend photon residence time, one dimensional nanostructures facilitate anisotropic charge transport and core shell or yolk shell configurations provide structurally confined reaction domains that stabilize the desired charge transfer pathways. The cumulative effect of these innovations is a distinct improvement in both photocatalytic activity and material stability.

Despite these advances, the practical implementation of bismuth based ternary heterostructures is constrained by several unresolved issues. Most available studies are carried out in simplified laboratory matrices that do not reflect the complexity of real wastewater environments. Actual effluents contain competing ions, turbidity, organic mixtures and fluctuating chemical conditions that influence photocatalyst activity and the nature of degradation intermediates. Furthermore, the ecological impacts of these materials are rarely assessed. Potential leaching of bismuth, halides, sulfides or silver containing components, as well as the generation of unintended transformation products, raises concerns about secondary pollution. A comprehensive assessment of leaching behavior, chronic toxicity and biodegradability of intermediates is necessary to guide safe deployment.

The mechanistic understanding of charge transfer in ternary systems also requires significant refinement. Many proposed mechanisms rely on indirect interpretations of photoluminescence, transient photocurrent or quencher trapping data. These methods do not fully capture the complexity of charge interactions in systems where three components contribute simultaneously. There is a need for more rigorous validation using time resolved spectroscopies, operando surface characterization and computational modelling. Consistent reporting of photon normalised metrics such as apparent quantum yield or external quantum efficiency is also essential since differences in irradiation intensity, wavelength distribution and reactor geometry often obscure meaningful comparison across studies.

Scalability and sustainable synthesis remain critical limitations. Although methods such as hydrothermal processing offer precise control

over crystallinity and morphology, they are not easily translated to industrial scales and often rely on high temperature treatments or hazardous solvents. Greener and more scalable routes such as sol gel synthesis, electrospinning, molten salt synthesis and spray pyrolysis present promising alternatives but require improved reproducibility and simplified processing. Future research must increasingly incorporate the principles of green chemistry by reducing solvent use, lowering thermal budgets and avoiding toxic or precious elements.

There is also a strong need to transition from powdered materials toward immobilized photocatalysts that can operate effectively in continuous flow systems. Embedding ternary heterostructures within membranes, polymeric fibers, ceramic supports or structured monoliths can reduce agglomeration, improve catalyst recovery and enable long term operation under real water conditions. These configurations also facilitate multifunctional treatment processes. Several bismuth based ternary systems have already demonstrated activity in hydrogen evolution, carbon dioxide reduction and microbial inactivation, suggesting a pathway toward integrated water purification and energy recovery strategies.

Finally, data driven approaches, including machine learning and computational screening, hold considerable promise for identifying optimal material combinations, predicting band structures and narrowing the vast compositional space of possible ternary systems. Together with long term pilot demonstrations, techno economic analyses and life cycle assessments, these tools will be essential for guiding the transition of bismuth based ternary photocatalysts from laboratory demonstrations to viable environmental technologies.

In summary, bismuth based ternary heterostructured photocatalysts possess unique structural and electronic attributes that make them highly effective candidates for the visible light degradation of organic pollutants. Their future development must be guided by a holistic perspective that balances photocatalytic efficiency with stability, environmental safety, sustainable synthesis and realistic operational performance. When these challenges are addressed through coordinated scientific and engineering efforts, these materials have the potential to evolve into impactful, sustainable and scalable solutions for global water purification.

CRediT authorship contribution statement

Benjamin O. Orimolade: Writing – review & editing, Writing – original draft, Methodology, Investigation, Data curation, Conceptualization. **Moses G. Peleyeju:** Writing – review & editing, Writing – original draft, Visualization, Methodology. **Tunde Lewis Yusuf:** Writing – review & editing, Writing – original draft, Resources, Investigation, Conceptualization.

Declaration of competing interest

The authors declare that they have no known competing financial interests or personal relationships that could have appeared to influence the work reported in this paper.

Data availability

No data was used for the research described in the article.

References

Akter, J., Juwon, J., Taesung, J., Gyu, K.J., Lee, H., 2020. Contamination assessment of pollutants and sediments of abandoned mines using integrated pollution index (IPI). Desalin. Water Treat. 200, 383–389. https://doi.org/10.5004/dwt.2020.26119.

Algarni, Z., Sultan Aljibori, H.S., Amari, A., Jasim, D.J., Diab, M.A., El-Sabban, H.A., Elboughdiri, N., Atamurotov, F., 2024. Photocatalytic hydrogen production and sulfamerazine degradation via a novel dual S-scheme photocatalyst: nanocomposite synthesis, characterization and mechanism insights. J. Water Process Eng. 68, 106402. https://doi.org/10.1016/j.jwpe.2024.106402.

Alnaggar, G., Hezam, A., Drmosh, Q.A., Ananda, S., 2021. Sunlight-driven activation of peroxymonosulfate by microwave synthesized ternary MoO3/Bi2O3/g-C3N4 heterostructures for boosting tetracycline hydrochloride degradation. Chemosphere 272, 129807. https://doi.org/10.1016/j.chemosphere.2021.129807.

Alomayri, T., 2025. Enhanced interfacial charge transfer in BiVO4/rGO/FeVO4 heterojunction composite for improved photocatalysis water purification. Ceram. Int. 51, 10193–10199. https://doi.org/10.1016/j.ceramint.2024.12.450.

Alsukaibi, A.K.D., 2022. Various approaches for the detoxification of toxic dyes in wastewater. Processes 10, 1968. https://doi.org/10.3390/pr10101968.

Ardila-Leal, L.D., Poutou-Piñales, R.A., Pedroza-Rodríguez, A.M., Quevedo-Hidalgo, B.E., 2021. A brief history of colour, the environmental impact of synthetic dyes and removal by using laccases. Molecules 26, 3813. https://doi.org/10.3390/molecules26133813.

Arman, N.Z., Salmiati, S., Aris, A., Salim, M.R., Nazifa, T.H., Muhamad, M.S., Marpongahtun, M., 2021. A review on emerging pollutants in the water environment: existences, health effects and treatment processes. Water 13, 3258. https://doi.org/10.3390/w13223258.

Asadpoor, R., Habibi, D., Aghababaei, N., 2025. Integrated dual Z-scheme n-n-p/Schottky junctions upon Ni-ZnO/Bi2WO6/PANI for increased photocatalytic ciprofloxacin degradation under visible light. Sep. Purif. Technol. 363, 132060. https://doi.org/10.1016/j.seppur.2025.132060.

Athar, M.S., Muneer, M., 2024. Construction of visible light responsive GO-stimulated In2O3/BiVO4 Z-scheme heterostructure: photocatalytic degradation of dye & antibiotics, anticancer activity and toxicity elimination. J. Alloys Compd. 980, 173385. https://doi.org/10.1016/j.jallcom.2023.173385.

Balapure, A., Ray Dutta, J., Ganesan, R., 2024. Recent advances in semiconductor heterojunctions: a detailed review of the fundamentals of photocatalysis, charge transfer mechanism and materials. RSC Appl. Interfaces 1, 43–69. https://doi.org/10.1039/D3LF00126A.

Banyal, R., sudhaik, A., kumar, R., Sonu, Raizada, P., Ahamad, T., Kaya, S., Maslov, M. M., Chaudhary, V., Hussain, C.M., Singh, P., 2024. Construction of novel BiOI/CuInS2/ZnO dual S-scheme charge transfer pathway for efficient antibiotic degradation. J. Phys. Chem. Solids 195. https://doi.org/10.1016/j.jpcs.2024.112132.

Ben Saber, N., Mezni, A., Alrooqi, A., Altalhi, T., 2020. A review of ternary nanostructures based noble metal/semiconductor for environmental and renewable energy applications. J. Mater. Res. Technol. 9, 15233–15262. https://doi.org/10.1016/j.jmrt.2020.10.090.

Bera, S.P., Godhaniya, M., Kothari, C., 2022. Emerging and advanced membrane technology for wastewater treatment: a review. J. Basic Microbiol. 62, 245–259. https://doi.org/10.1002/jobm.202100259.

Cai, M., He, C., Yu, H., Shui, A., 2024. Fabrication of the ternary dual S-scheme ZnO/ZnS/In2S3 heterojunction for enhancing pollutant photodegradation. Appl. Surf. Sci. 652, 159284. https://doi.org/10.1016/j.apsusc.2023.159284.

Cao, S., Li, J., Wu, L., Mao, X., Zou, S., Li, Y., Da, K., Yang, J., Fan, X., 2024. Synthesis and photocatalytic mechanism study of visible light-driven Z-type Ag/AgBr/Bi2MoO6 composite materials for efficient degradation of organic dyes. J. Mol. Struct. 1317, 139137. https://doi.org/10.1016/j.molstruc.2024.139137.

Chawla, A., Sudhaik, A., Sonu, Kumar, R., Raizada, P., Ahamad, T., Khan, A.A.P., Van Le, Q., Nguyen, V.-H., Thakur, S., Singh, P., 2025. Bi2S3-based photocatalysts: properties, synthesis, modification strategies, and mechanistic insights towards environmental sustainability and green energy technologies. Coord. Chem. Rev. 529, 216443. https://doi.org/10.1016/j.ccr.2025.216443.

Chen, J., Qin, S., Yang, X., Wang, Y., Yang, T., Que, M., Ma, Y., Li, Y., 2024. Synthesis of highly conductive carbon quantum dot-enhanced Z-scheme BiOBr/g-C3N4 heterojunction for effective photocatalytic degradation of tetracycline hydrochloride. J. Phys. Chem. Solids 189, 111957. https://doi.org/10.1016/j.jpcs.2024.111957.

Chen, Z.J., Guo, H., Liu, H.Y., Niu, C.G., Huang, D.W., Yang, Y.Y., Liang, C., Li, L., Li, J. C., 2022. Construction of dual S-scheme Ag2CO3/Bi4O5I2/g-C3N4 heterostructure photocatalyst with enhanced visible-light photocatalytic degradation for tetracycline. Chem. Eng. J. 438. https://doi.org/10.1016/j.cej.2022.135471.

Cho, E.C., Hsiao, Y.S., Huang, J.H., Sung, M.Y., Chen, Y.L., Wu, N.J., Hsu, S.C., Weng, H. C., Lee, K.C., 2023. Construction of BiVO4/Bi2WO6/WO3 heterojunctions with improved photocatalytic capability in elimination of dye and antibiotics and inactivation of E. coli. J. Taiwan Inst. Chem. Eng. 149, 104991. https://doi.org/10.1016/j.jtice.2023.104991.

Chowdhury, A.P., Anantharaju, K.S., Umare, S.S., Dhar, S.S., 2022. Facile fabrication of binary BiOCl-Cu2CoSnS4 and ternary BiOCl-Cu2CoSnS4-TiO2 heterojunction nano photocatalyst for efficient sunlight-driven removal of direct blue 71 in an aqueous medium. Colloids Surfaces A Physicochem. Eng. Asp. 652, 129841. https://doi.org/10.1016/j.colsurfa.2022.129841.

Cui, S., Cong, Y., Zhao, W., Guo, R., Wang, X., Lv, B., Liu, H., Liu, Y., Zhang, Q., 2024. A novel multifunctional magnetically recyclable BiOBr/ZnFe2O4-GO S-scheme ternary heterojunction: photothermal synergistic catalysis under Vis/NIR light and NIR-driven photothermal detection of tetracycline. J. Colloid Interface Sci. 654, 356–370. https://doi.org/10.1016/j.jcis.2023.10.051.

Cui, Y., Nengzi, L. chao, Gou, J., Huang, Y., Li, B., Cheng, X., 2020. Fabrication of dual Z-scheme MIL-53(Fe)/A-Bi2O3/g-C3N4 ternary composite with enhanced visible light photocatalytic performance. Sep. Purif. Technol. 232. https://doi.org/10.1016/j.seppur.2019.115959.

D, R.D., T, S., R.M, M., D, P., P, M.Y.A., S.M, A.K., R, R., 2024. A novel photocatalytic activity of Bi2S3 nanoparticles for pharmaceutical and organic pollution removal in water remediation. Chem. Phys. Impact 8, 100605. https://doi.org/10.1016/j.chphi.2024.100605.

Dang, J., Guo, J., Wang, L., Guo, F., Shi, W., Li, Y., Guan, W., 2022. Construction of Z-scheme Fe3O4/BiOCl/BiOI heterojunction with superior recyclability for improved photocatalytic activity towards tetracycline degradation. J. Alloys Compd. 893, 162251. https://doi.org/10.1016/j.jallcom.2021.162251.

Das, K., Bariki, R., Majhi, D., Mishra, A., Das, K.K., Dhiman, R., Mishra, B.G., 2022. Facile synthesis and application of CdS/Bi20TiO32/Bi4Ti3O12 ternary heterostructure: a synergistic multi-heterojunction photocatalyst for enhanced endosulfan degradation and hydrogen evolution reaction. Appl. Catal. B Environ. 303, 120902. https://doi.org/10.1016/j.apcatb.2021.120902.

Dhillon, M., Naskar, A., Kaushal, N., Bhansali, S., Saha, A., Basu, A.K., 2024. A novel GO hoisted SnO2-BiOBr bifunctional catalyst for the remediation of organic dyes under illumination by visible light and electrocatalytic water splitting. Nanoscale 16, 12445–12458. https://doi.org/10.1039/d4nr01154f.

Ding, J., Li, C., Yin, H., Zhou, Y., Wang, S., Liu, K., Li, M., Wang, J., 2023. One-pot solvothermal synthesis of Bi/Bi2S3/Bi2WO6 S-scheme heterojunction with enhanced photoactivity towards antibiotic oxytetracycline degradation under visible light. Environ. Pollut. 327, 121550. https://doi.org/10.1016/j.envpol.2023.121550.

Drmosh, Q.A., Hezam, A., Hendi, A.H.Y., Qamar, M., Yamani, Z.H., Byrappa, K., 2020. Ternary Bi2S3/MoS2/TiO2 with double Z-scheme configuration as high performance photocatalyst. Appl. Surf. Sci. 499. https://doi.org/10.1016/j.apsusc.2019.143938.

Finlayson, A.P., Tsaneva, V.N., Lyons, L., Clark, M., Glowacki, B.A., 2006. Evaluation of Bi-W-oxides for visible light photocatalysis. phys. stat. sol. 203, 327–335. https://doi.org/10.1002/pssa.200521129.

Fu, S., Huang, Q., Deng, P., Liu, Z., Zhang, X., Zhu, H., Zhou, J., 2021. Novel hierarchical BiOBr-based photocatalyst co-modified with Ag nanoparticles and porous g-C3N4 nanosheets for efficient removal of tetracycline and Cr(VI). J. Mater. Sci. Mater. Electron. 32, 13014–13028. https://doi.org/10.1007/s10854-021-05653-8.

Fujishima, A., Zhang, X., Tryk, D.A., 2008. TiO2 photocatalysis and related surface phenomena. Surf. Sci. Rep. 63, 515–582. https://doi.org/10.1016/j.surfrep.2008.10.001.

Gao, B., Pan, Y., Chang, Q., Xi, Z., Yang, H., 2022a. Hierarchically Z-scheme photocatalyst of {0 1 0}BiVO4/Ag/CdS with enhanced performance in synergistic adsorption-photodegradation of fluoroquinolones in water. Chem. Eng. J. 435. https://doi.org/10.1016/j.cej.2022.134834.

Gao, B., Pan, Y., Yang, H., 2022b. Enhanced photo-Fenton degradation of fluoroquinolones in water assisted by a 3D composite sponge complexed with a S-scheme MoS2/Bi2S3/BiVO4 ternary photocatalyst. Appl. Catal. B Environ. 315, 121580. https://doi.org/10.1016/j.apcatb.2022.121580.

Gao, H., Zhao, X., Zhang, H., Chen, J., Wang, S., Yang, H., 2020. Construction of 2D/0D/2D face-to-face contact g-C3N4@Au@Bi4Ti3O12 heterojunction photocatalysts for degradation of rhodamine B. J. Electron. Mater. 49, 5248–5259. https://doi.org/10.1007/s11664-020-08243-2.

Gao, Q., Wang, Z., Li, J., Liu, B., Liu, C., 2022. Facile synthesis of ternary dual z−scheme g−C3N4/Bi2MoO6/CeO2 photocatalyst with enhanced 4–chlorophenol removal: degradation pathways and mechanism. Environ. Pollut. 315, 120436. https://doi.org/10.1016/j.envpol.2022.120436.

Ghorbani, M., Solaimany Nazar, A.R., Frahadian, M., Tangestaninejad, S., 2023. Fabrication of novel ZnO@BiOBr/UiO-66-NH2 core-shell heterojunction for improved tetracycline degradation. Appl. Surf. Sci. 612, 155819. https://doi.org/10.1016/j.apsusc.2022.155819.

Guan, Z., Li, X., Wu, Y., Chen, Z., Huang, X., Wang, D., Yang, Q., Liu, J., Tian, S., Chen, X., Zhao, H., 2021. AgBr nanoparticles decorated 2D/2D GO/Bi2WO6 photocatalyst with enhanced photocatalytic performance for the removal of tetracycline hydrochloride. Chem. Eng. J. 410, 128283. https://doi.org/10.1016/j.cej.2020.128283.

Guo, J., Yang, C., Sun, Z., Yang, Z., Wang, L., Lu, C., Ma, Z., Guo, F., 2020. Ternary Fe3O4/MoS2/BiVO4 nanocomposites: novel magnetically separable visible light-driven photocatalyst for efficiently degradation of antibiotic wastewater through p–n heterojunction. J. Mater. Sci. Mater. Electron. 31, 16746–16758. https://doi.org/10.1007/s10854-020-04230-9.

Han, H., Xu, Y., Cheng, Y., Tang, L., Jin, J., Liu, X., Ma, C., Lu, Z., 2025. Frustrated Lewis pairs in CO2 photoreduction: a review on synergistic activation and charge separation. Chinese J. Struct. Chem. 44, 100728. https://doi.org/10.1016/j.cjsc.2025.100728.

Hong, X., Li, Y., Wang, X., Long, J., Liang, B., 2022. Carbon nanosheet/MnO2/BiOCl ternary composite for degradation of organic pollutants. J. Alloys Compd. 891, 162090. https://doi.org/10.1016/j.jallcom.2021.162090.

Hosseinzadeh, G., Zinatloo-Ajabshir, S., Yousefi, A., 2022. Innovative synthesis of a novel ZnO/ZnBi2O4/graphene ternary heterojunction nanocomposite photocatalyst in the presence of tragacanth mucilage as natural surfactant. Ceram. Int. 48, 6078–6086. https://doi.org/10.1016/j.ceramint.2021.11.146.

Hou, J., Xie, Y., Sun, Y., Kuang, Y., Jiao, Z., Wang, Q., 2022. Construction of a double Z-scheme Bi2O3–CuBi2O4–CuO composite photocatalyst for the enhanced photocatalytic activity. Ceram. Int. 48, 20648–20657. https://doi.org/10.1016/j.ceramint.2022.04.034.

Hu, G., Ren, X., Meng, D., Gao, D., Guo, Q., Hu, X., Wang, L., Song, J., 2023. Facile fabrication of S-scheme Bi2MoO6/g-C3N4/sepiolite ternary photocatalyst for efficient tetracycline degradation under visible light. Mater. Sci. Semicond. Process. 166, 107712. https://doi.org/10.1016/j.mssp.2023.107712.

Hu, H., Kong, W., Wang, J., Liu, C., Cai, Q., Kong, Y., Zhou, S., Yang, Z., 2021. Engineering 2D compressed layered g-C3N4 nanosheets by the intercalation of BiVO4-Bi2WO6 composites for boosting photocatalytic activities. Appl. Surf. Sci. 557, 149796. https://doi.org/10.1016/j.apsusc.2021.149796.

Hu, K., Chen, C., Zhu, Y., Zeng, G., Huang, B., Chen, W., Liu, S., Lei, C., Li, B., Yang, Y., 2019. Ternary Z-scheme heterojunction of Bi 2 WO 6 with reduced graphene oxide (rGO) and meso-tetra (4-carboxyphenyl) porphyrin (TCPP) for enhanced visible-light photocatalysis. J. Colloid Interface Sci. 540, 115–125. https://doi.org/10.1016/j.jcis.2019.01.013.

Huang, L., Liu, H., Wang, Y., Zhang, T.C., Yuan, S., 2023. Construction of ternary Bi2O3/biochar/g-C3N4 heterojunction to accelerate photoinduced carrier separation for enhanced tetracycline photodegradation. Appl. Surf. Sci. 616, 156509. https://doi.org/10.1016/j.apsusc.2023.156509.

Huang, W.L., Zhu, Q., 2009. DFT calculations on the electronic structures of BiOX (X = F, Cl, Br, I) photocatalysts with and without semicore Bi 5d states. J. Comput. Chem. 30, 183–190. https://doi.org/10.1002/jcc.21055.

Huang, Z., Zhu, P., Zhang, S., Duan, M., Liu, M., Li, X., 2024. Synthesis of double Z-type heterojunction AgI/Ag6Si2O7/BiOI photocatalyst for antibiotics degradation and weakening toxicity. J. Environ. Chem. Eng. 12, 113432. https://doi.org/10.1016/j.jece.2024.113432.

Hussain, A., Hou, J., Tahir, M., Ali, S., Rehman, Z.U., Bilal, M., Zhang, T., Dou, Q., Wang, X., 2024. Recent advances in BiOX-based photocatalysts to enhanced efficiency for energy and environment applications. Catal. Rev. 66, 119–173. https://doi.org/10.1080/01614940.2022.2041836.

Jabbar, Z.H., Graimed, B.H., Okab, A.A., Ammar, S.H., Majdi, A., 2025. Promoting the photocatalytic capacity of type I heterojunction (Bi12O17Cl2/Sb2O3) by incorporating MWCNTs for boosted carbamazepine degradation mechanism. Opt. Mater. 162, 116883. https://doi.org/10.1016/j.optmat.2025.116883.

Jabbar, Z.H., Okab, A.A., Graimed, B.H., Issa, M.A., Ammar, S.H., 2023. Photocatalytic destruction of Congo red dye in wastewater using a novel Ag2WO4/Bi2S3 nanocomposite decorated g-C3N4 nanosheet as ternary S-scheme heterojunction: improving the charge transfer efficiency. Diam. Relat. Mater. 133, 109711. https://doi.org/10.1016/j.diamond.2023.109711.

Ji, W., Xiao, Y., Xiao, F., Li, L., Chen, M., Wang, H., 2024. A novel multifunctional photocatalytic membrane based on ternary heterojunction TiO2@PDA@BiOBr for biochemical oily wastewater purification. Chem. Eng. J. 493, 152759. https://doi.org/10.1016/j.cej.2024.152759.

Jia, Y., Li, J., Liu, Z., Wang, Q., Zhang, W., Bae, J.S., Liu, C., 2022. Pt-GdCrO3-Bi2MoO6 ternary heterojunction with high photocatalytic activities for CO2 reduction and water purification. Chem. Eng. J. 437, 135300. https://doi.org/10.1016/j.cej.2022.135300.

Jiang, H., Xing, Z., Li, Z., Pan, K., Yang, Z., Wang, K., Guo, M., Yang, S., Zhou, W., 2020. Wide-spectrum response urchin-like Bi2S3 spheres and ZnS quantum dots co-decorated mesoporous g-C3N4 nanosheets heterojunctions for promoting charge separation and enhancing photothermal-photocatalytic performance. Appl. Surf. Sci. 527, 146653. https://doi.org/10.1016/j.apsusc.2020.146653.

Jiang, J., Wei, Y., Chen, J., Dai, J., Ma, J., Qiang, L., Xue, J., Liu, W., 2024. Photocatalytic degradation of antibiotics using a Li-C3N4/ZnO/BiOI: insights on the electron transport pathways. J. Taiwan Inst. Chem. Eng. 155, 105293. https://doi.org/10.1016/j.jtice.2023.105293.

Jiang, X., Kong, D., Luo, B., Wang, M., Zhang, D., Pu, X., 2022. Preparation of magnetically retrievable flower-like AgBr/BiOBr/NiFe2O4 direct Z-scheme heterojunction photocatalyst with enhanced visible-light photoactivity. Colloids Surfaces A Physicochem. Eng. Asp. 633, 127880. https://doi.org/10.1016/j.colsurfa.2021.127880.

Jin, K., Qin, M., Li, X., Wang, R., Zhao, Y., Wang, H., 2022. Z-scheme Au@TiO2/Bi2WO6 heterojunction as efficient visible-light photocatalyst for degradation of antibiotics. J. Mol. Liq. 364, 120017. https://doi.org/10.1016/j.molliq.2022.120017.

Jurado, A., Pujades, E., Walther, M., Diaz-Cruz, M.S., 2022. Occurrence, fate, and risk of the organic pollutants of the surface water watch list in European groundwaters: a review. Environ. Chem. Lett. 20, 3313–3333. https://doi.org/10.1007/s10311-022-01441-w.

Kan, L., Mu, W., Chang, C., Lian, F., 2023. Dual S-scheme graphitic carbon-doped α-Bi2O3/β-Bi2O3/Bi5O7I ternary heterojunction photocatalyst for the degradation of Bisphenol A. Sep. Purif. Technol. 312, 123388. https://doi.org/10.1016/j.seppur.2023.123388.

Kanakaraju, D., Glass, B.D., Oelgemöller, M., 2018. Advanced oxidation process-mediated removal of pharmaceuticals from water: a review. J. Environ. Manage. 219, 189–207. https://doi.org/10.1016/j.jenvman.2018.04.103.

Kang, J., Jin, C., Li, Z., Wang, M., Chen, Z., Wang, Y., 2020. Dual Z-scheme MoS2/g-C3N4/Bi24O31Cl10 ternary heterojunction photocatalysts for enhanced visible-light photodegradation of antibiotic. J. Alloys Compd. 825, 153975. https://doi.org/10.1016/j.jallcom.2020.153975.

Karpińska, J., Kotowska, U., 2019. Removal of organic pollution in the water environment. Water (Switzerland) 11. https://doi.org/10.3390/w11102017.

Kausar, F., Varghese, A., Pinheiro, D., Devi, K.R.S., 2022. Recent trends in photocatalytic water splitting using titania based ternary photocatalysts-A review. Int. J. Hydrogen Energy 47, 22371–22402. https://doi.org/10.1016/j.ijhydene.2022.05.058.

Khan, H.K., Rehman, M.Y.A., Junaid, M., Lv, M., Yue, L., Haq, I., Xu, N., Malik, R.N., 2022. Occurrence, source apportionment and potential risks of selected PPCPs in groundwater used as a source of drinking water from key urban-rural settings of Pakistan. Sci. Total Environ. 807, 151010. https://doi.org/10.1016/j.scitotenv.2021.151010.

Kim, J.H., Lee, J.S., 2019. Elaborately modified BiVO4 photoanodes for solar water splitting. Adv. Mater. 31, 1–35. https://doi.org/10.1002/adma.201806938.

Kohantorabi, M., Moussavi, G., Oulego, P., Giannakis, S., 2021. Radical-based degradation of sulfamethoxazole via UVA/PMS-assisted photocatalysis, driven by magnetically separable Fe3O4@CeO2@BiOI nanospheres. Sep. Purif. Technol. 267, 118665. https://doi.org/10.1016/j.seppur.2021.118665.

Kumar, A., Sharma, S.K., Sharma, G., Al-Muhtaseb, A.H., Naushad, M., Ghfar, A.A., Stadler, F.J., 2019a. Wide spectral degradation of Norfloxacin by Ag@BiPO4/BiOBr/BiFeO3 nano-assembly: elucidating the photocatalytic mechanism under different

light sources. J. Hazard. Mater. 364, 429–440. https://doi.org/10.1016/j.jhazmat.2018.10.060.
Kumar, A., Sharma, S.K., Sharma, G., Al-Muhtaseb, A.H., Naushad, M., Ghfar, A.A., Stadler, F.J., 2019b. Wide spectral degradation of Norfloxacin by Ag@BiPO4/BiOBr/BiFeO3 nano-assembly: elucidating the photocatalytic mechanism under different light sources. J. Hazard. Mater. 364, 429–440. https://doi.org/10.1016/j.jhazmat.2018.10.060.
Kurwadkar, S., 2019. Occurrence and distribution of organic and inorganic pollutants in groundwater. Water Environ. Res. 91, 1001–1008. https://doi.org/10.1002/wer.1166.
Lee, D., Gibson, J.M., Brown, J., Habtewold, J., Murphy, H.M., 2023. Burden of disease from contaminated drinking water in countries with high access to safely managed water: a systematic review. Water Res. 242, 120244. https://doi.org/10.1016/j.watres.2023.120244.
Li, F., Zhu, G., Jiang, J., Yang, L., Deng, F., Arramel, Li, X., 2024. A review of updated S-scheme heterojunction photocatalysts. J. Mater. Sci. Technol. 177, 142–180. https://doi.org/10.1016/j.jmst.2023.08.038.
Li, H., Chen, Y., Zhou, W., Jiang, H., Liu, H., Chen, X., Guohui, T., 2019. WO3/BiVO4/BiOCl porous nanosheet composites from a biomass template for photocatalytic organic pollutant degradation. J. Alloys Compd. 802, 76–85. https://doi.org/10.1016/j.jallcom.2019.06.187.
Li, J., Yuan, H., Zhang, W., Jin, B., Feng, Q., Huang, J., Jiao, Z., 2022. Advances in z-scheme semiconductor photocatalysts for the photoelectrochemical applications: a review. Carbon Energy 4, 294–331. https://doi.org/10.1002/cey2.179.
Li, N., Niu, Y., An, W., Liu, Z., Ruan, F., Fan, G., 2024. Unraveling charge transfer dynamics in AgBr/Bi4Ti3O12/Bi2Sn2O7 ternary S-scheme heterojunction photocatalyst. J. Colloid Interface Sci. 669, 175–189. https://doi.org/10.1016/j.jcis.2024.04.216.
Li, Y., Jinping, A.E., Ae, L., Huang, X., 2008. Synthesis and visible-light photocatalytic property of Bi 2 WO 6 hierarchical octahedron-like structures. Nanoscale Res. Lett. 3, 365–371. https://doi.org/10.1007/s11671-008-9168-7.
Li, Y., Wang, H., Xie, J., Hou, J., Song, X., Dionysiou, D.D., 2021. Bi2WO6-TiO2/starch composite films with Ag nanoparticle irradiated by γ-ray used for the visible light photocatalytic degradation of ethylene. Chem. Eng. J. 421, 129986. https://doi.org/10.1016/j.cej.2021.129986.
Li, Z., Shen, D., Hu, X., Yang, X., Li, Y., Bao, M., 2023. An S-scheme NH2-MIL-101(Fe)@MCN/Bi2O3 heterojunction photocatalyst for the degradation of tetracycline and production of H2O2. Chemosphere 343, 140234. https://doi.org/10.1016/j.chemosphere.2023.140234.
Liang, Y., Li, W., Wang, X., Zhou, R., Ding, H., 2022. TiO2–ZnO/Au ternary heterojunction nanocomposite: excellent antibacterial property and visible-light photocatalytic hydrogen production efficiency. Ceram. Int. 48, 2826–2832. https://doi.org/10.1016/j.ceramint.2021.10.072.
Lin, H., Hassan, W.H., Abbood, H.A., Samad, S., Yang, C., Diab, M.A., El-Sabban, H.A., Jumanazarov, D., Atamurotov, F., Samandarov, B., Zhu, P., 2025. Designing a novel Ti3C2 MXene-bridged Z-scheme photocatalyst for effective H2 generation and removal of non-biodegradable norfloxacin: optimization and mechanism insights. J. Alloys Compd. 1031, 181029. https://doi.org/10.1016/j.jallcom.2025.181029.
Lin, Z., Xu, J., Gu, H., Huang, J., Lin, J., Shao, J., Wang, D., Li, H., 2023. A review on research progress in photocatalytic degradation of organic pollutants by Bi2MoO6. J. Environ. Chem. Eng. 11, 110911. https://doi.org/10.1016/j.jece.2023.110911.
Lotfy, H.R., Roubík, H., 2023. Water purification using activated carbon prepared from agriculture waste — overview of a recent development. Biomass Convers. Biorefinery 13, 15577–15590. https://doi.org/10.1007/s13399-021-01618-3.
Low, J., Yu, J., Jaroniec, M., Wageh, S., Al-Ghamdi, A.A., 2017. Heterojunction photocatalysts. Adv. Mater. https://doi.org/10.1002/adma.201601694.
Lu, Z., Zhou, G., Li, B., Xu, Y., Wang, P., Yan, H., Song, M., Ma, C., Han, S., Liu, X., 2022. Heterotopic reaction strategy for enhancing selective reduction and synergistic oxidation ability through trapping Cr (VI) into specific reaction site: a stable and self-cleaning ion imprinted CdS/HTNW photocatalytic membrane. Appl. Catal. B Environ. 301, 120787. https://doi.org/10.1016/j.apcatb.2021.120787.
Luo, H., Dong, S., Li, H., Chen, S., Huang, J., Xu, K., 2023. Novel dual S-scheme BiOI/AgI/Bi2WO6 heterojunction with enhanced photocatalytic activity for highly efficient removal of organic pollutants. Opt. Mater. 140, 113842. https://doi.org/10.1016/j.optmat.2023.113842.
Luo, H., Yan, M., Wu, Y., Lin, X., Yan, Y., 2021. Facile synthesis of PVDF photocatalytic membrane based on NCQDs/BiOBr/TiO2 heterojunction for effective removal of tetracycline. Mater. Sci. Eng. B 265, 114996. https://doi.org/10.1016/j.mseb.2020.114996.
Luo, J., Shi, Z., Meng, J., Li, F., Li, T., Zhang, M., Greco, R., Cao, W., 2023. Z-scheme Bi2O3/Bi/ZnIn2S4 photocatalyst for enhancing the removal performance of Cr(VI), 2,4-dinitrophenol and tetracycline. J. Ind. Eng. Chem. 124, 250–262. https://doi.org/10.1016/j.jiec.2023.04.014.
Lv, C.N., Zhang, L., Hu, J.S., Huang, X.H., Hou, C.M., 2019. Band engineering of Ag-Bi12GeO20-Bi2WO6 composite photocatalyst: interface regulation and enhanced photocatalytic performance. Ceram. Int. 45, 5249–5258. https://doi.org/10.1016/j.ceramint.2018.11.222.
Ma, Q., Ren, J., Sun, X., Chen, X., Liu, G., Wang, S., Yang, H., 2025. Strong evidence for interface-field-induced photocarrier separation in new AgFeO2-BiVO4 heterostructures and their efficient photo-Fenton degradation of ciprofoxacin. Appl. Surf. Sci. 679, 161275. https://doi.org/10.1016/j.apsusc.2024.161275.
Macêdo, W.V., Madsen, J.S., Schacksen, P., Sandeep, R., Nielsen, J.L., Biller, P., Vergeynst, L., 2025. Aerobic biological treatment of hydrothermal liquefaction process water of sewage sludge: nitrification inhibition and removal of hazardous pollutants. Water Res. 277, 123351. https://doi.org/10.1016/j.watres.2025.123351.
Majhi, D., Kumar Mishra, A., Das, K., Bariki, R., Mishra, B.G., 2021. Plasmonic Ag nanoparticle decorated Bi2O3/CuBi2O4 photocatalyst for expeditious degradation of 17α-ethinylestradiol and Cr(VI) reduction: insight into electron transfer mechanism and enhanced photocatalytic activity. Chem. Eng. J. 413. https://doi.org/10.1016/j.cej.2020.127506.
Maynez-Navarro, O.D., Sánchez-Salas, J.L., 2018. Focus on Zinc oxide as a photocatalytic material for water treatment. Int J Biorem Biodegrad 106, 1–10. https://doi.org/10.29011/IJBB-106/100006.
Mirhosseini, H., Mostafavi, A., Shamspur, T., Sargazi, G., 2022. Fabrication of an efficient ternary TiO2/Bi2WO6 nanocomposite supported on g-C3N4 with enhanced visible-light- photocatalytic activity: modeling and systematic optimization procedure. Arab. J. Chem. 15, 103729. https://doi.org/10.1016/j.arabjc.2022.103729.
Mohana Roopan, S., Khan, M.A., 2023. MoS 2 based ternary composites: review on heterogeneous materials as catalyst for photocatalytic degradation. Catal. Rev. 65, 620–693. https://doi.org/10.1080/01614940.2021.1962493.
Morshedy, A.S., El-Fawal, E.M., Zaki, T., El-Zahhar, A.A., Alghamdi, M.M., El Naggar, A. M.A., 2024. A review on heterogeneous photocatalytic materials: mechanism, perspectives, and environmental and energy sustainability applications. Inorg. Chem. Commun. 163, 112307. https://doi.org/10.1016/j.inoche.2024.112307.
Nie, C., Wang, X., Lu, P., Zhu, Y., Li, X., Tang, H., 2024. Advancements in S-scheme heterojunction materials for photocatalytic environmental remediation. J. Mater. Sci. Technol. 169, 182–198. https://doi.org/10.1016/j.jmst.2023.06.011.
Nkinda, M.S., Rwiza, M.J., Ijumba, J.N., Njau, K.N., 2021. Heavy metals risk assessment of water and sediments collected from selected river tributaries of the Mara river in Tanzania. Discov. Water 1, 1–19. https://doi.org/10.1007/s43832-021-00003-5.
Ofiera, L.M., Wintgens, T., Kazner, C., 2025. Comparative analysis of conventional and modified constructed wetlands for the removal of trace organic compounds from municipal wastewater effluent. Sci. Total Environ. 987, 179796. https://doi.org/10.1016/j.scitotenv.2025.179796.
Oluwasina, O.O., Adelodun, A.A., 2024. Recent advances in remediating organic-laden wastewater using graphene-based nanomaterials. Nanotechnol. Environ. Eng. 9, 389–409. https://doi.org/10.1007/s41204-024-00373-w.
Orimolade, B.O., Arotiba, O.A., 2020. Bismuth vanadate in photoelectrocatalytic water treatment systems for the degradation of organics: a review on recent trends. J. Electroanal. Chem. 878, 114724. https://doi.org/10.1016/j.jelechem.2020.114724.
Orimolade, B.O., Idris, A.O., Feleni, U., Mamba, B., 2021. Recent advances in degradation of pharmaceuticals using Bi 2 WO 6 mediated photocatalysis – a comprehensive review. Environ. Pollut. 289, 117891. https://doi.org/10.1016/j.envpol.2021.117891.
Orimolade, B.O., Koiki, B.A., Peleyeju, G.M., Arotiba, O.A., 2019. Visible light driven photoelectrocatalysis on a FTO/BiVO 4/BiOI anode for water treatment involving emerging pharmaceutical pollutants. Electrochim. Acta 307, 285–292. https://doi.org/10.1016/j.electacta.2019.03.217.
Orimolade, B.O., Oladipo, A.O., Idris, A.O., Usisipho, F., Azizi, S., Maaza, M., Lebelo, S. L., Mamba, B.B., 2023. Advancements in electrochemical technologies for the removal of fluoroquinolone antibiotics in wastewater: a review. Sci. Total Environ. 881, 163522. https://doi.org/10.1016/j.scitotenv.2023.163522.
Ozaki, N., Mao, Y., Kindaichi, T., Ohashi, A., 2025. Mass flow of PAHs and fragrance substances in the sedimentation tanks of conventional domestic wastewater treatment plant–trace organic chemicals passing through sedimentation tank. Clean. Water 3, 100074. https://doi.org/10.1016/j.clwat.2025.100074.
Paíga, P., Correia-Sá, L., Correia, M., Figueiredo, S., Vieira, J., Jorge, S., Silva, J.G., Delerue-Matos, C., 2024. Temporal analysis of pharmaceuticals as emerging contaminants in surface water and wastewater samples: a case Study. J. Xenobiotics 14, 873–892. https://doi.org/10.3390/jox14030048.
Peyrovi, M., Ghasemi, S., Khorasheh, F., 2025. Self-assembly of MIL-100(Fe)@Bi2WO6/g-C3N4 as a visible-light-responsive double Z-scheme heterojunction for the degradation of Reactive blue 4. Inorg. Chem. Commun. 178, 114625. https://doi.org/10.1016/j.inoche.2025.114625.
Pournemati, K., Habibi-Yangjeh, A., Khataee, A., 2022. Ternary novel TiO2/MgBi2O6/Bi2O3 nanocomposites with n-n-p heterojunctions: impressive visible-light-triggered photocatalytic degradation of tetracycline. Adv. Powder Technol. 33, 103820. https://doi.org/10.1016/j.apt.2022.103820.
Preeyanghaa, M., Dhileepan, M.D., Madhavan, J., Neppolian, B., 2022. Revealing the charge transfer mechanism in magnetically recyclable ternary g-C3N4/BiOBr/Fe3O4 nanocomposite for efficient photocatalytic degradation of tetracycline antibiotics. Chemosphere 303, 135070. https://doi.org/10.1016/j.chemosphere.2022.135070.
Qiu, Y., Zhang, Y., Chen, Z., Wang, X., Lu, T., Wang, Q., Zhan, Z., 2023. Dual Z-scheme heterojunction NH2-UiO-66/BiOBr/AgI with enhanced performance on visible light driven elimination of tetracycline and Cr(VI). Appl. Surf. Sci. 640, 158402. https://doi.org/10.1016/j.apsusc.2023.158402.
Qu, X., Liu, M., Li, L., Wang, R., Sun, H., Shi, L., Du, F., 2019. BiOBr flakes decoration and structural modification for CdTe/TiO 2 spheres: towards water decontamination under simulated light irradiation. Mater. Sci. Semicond. Process. 93, 331–338. https://doi.org/10.1016/j.mssp.2019.01.006.
Ren, M., Ao, Y., Wang, P., Wang, C., 2019. Construction of silver/graphitic-C3N4/bismuth tantalate Z-scheme photocatalyst with enhanced visible-light-driven performance for sulfamethoxazole degradation. Chem. Eng. J. 378, 122122. https://doi.org/10.1016/j.cej.2019.122122.
Saadati, A., Habibi-Yangjeh, A., Rahim Pouran, S., Yekan Motlagh, P., Khataee, A., 2023. Facile integration of brown TiO2−x with Bi4V2O11 and BiVO4: double S-scheme mechanism for exceptional visible-light photocatalytic performance in degradation of pollutants. Adv. Powder Technol. 34, 103956. https://doi.org/10.1016/j.apt.2023.103956.

Sabit, D.A., Ebrahim, S.E., 2023. Fabrication of magnetic BiOBr/ZnFe2O4/CuO heterojunction for improving the photocatalytic destruction of malachite green dye under LED irradiation: dual S-scheme mechanism. Mater. Sci. Semicond. Process. 163, 107559. https://doi.org/10.1016/j.mssp.2023.107559.

Saini, P., Goswami, A., Gaur, Y., Bhatt, E., 2025. Current advancements and emerging trends of nanoparticles as photocatalysts for treatment of dye wastewater. https://doi.org/10.1007/978-3-031-80189-1_2.

Sarkar, P., De, S., Neogi, S., 2022. Microwave assisted facile fabrication of dual Z-scheme g-C3N4/ZnFe2O4/Bi2S3 photocatalyst for peroxymonosulphate mediated degradation of 2,4,6-Trichlorophenol: the mechanistic insights. Appl. Catal. B Environ. 307, 121165. https://doi.org/10.1016/j.apcatb.2022.121165.

Sathya, K., Nagarajan, K., Carlin Geor Malar, G., Rajalakshmi, S., Raja Lakshmi, P., 2022. A comprehensive review on comparison among effluent treatment methods and modern methods of treatment of industrial wastewater effluent from different sources. Appl. Water Sci. 12, 70. https://doi.org/10.1007/s13201-022-01594-7.

Sharma, K., Sonu, Sudhaik, A., Ahamad, T., Kaya, S., Nguyen, L.H., Maslov, M.M., Le, Q. Van, Nguyen, V.H., Singh, P., Raizada, P., 2024. Unraveling the synergism mechanistic insight of O-vacancy and interfacial charge transfer in WO3-x decorated on Ag2CO3/BiOBr for photocatalysis of water pollutants: based on experimental and density functional theory (DFT) studies. Environ. Res. 260, 119610. https://doi.org/10.1016/j.envres.2024.119610.

Sharma, M., Kant, R., Sharma, A.K., Sharma, A.K., 2025. Exploring the impact of heavy metals toxicity in the aquatic ecosystem. Int. J. Energy Water Resour 9, 267–280. https://doi.org/10.1007/s42108-024-00284-1.

Shen, H., Yang, C., Xue, W., Hao, L., Wang, D., Fu, F., Sun, Z., 2023. Construction of ternary bismuth-based heterojunction by using (BiO) 2 CO 3 as electron bridge for highly efficient degradation of phenol. Chem. Eur J. 29, 202300748. https://doi.org/10.1002/chem.202300748.

Shoja, A., Habibi-Yangjeh, A., Mousavi, M., Ghosh, S., 2020. BiOBr and BiOCl decorated on TiO2 QDs: impressively increased photocatalytic performance for the degradation of pollutants under visible light. Adv. Powder Technol. 31, 3582–3596. https://doi.org/10.1016/j.apt.2020.07.002.

Som, I., Roy, M., Saha, R., 2020. Advances in nanomaterial-based water treatment approaches for photocatalytic degradation of water pollutants. ChemCatChem 12, 3409–3433. https://doi.org/10.1002/cctc.201902081.

Subhiksha, V., Okla, M.K., Alaraidh, I.A., Mohebaldin, A., Soufan, W., Abdel-Maksoud, M.A., Abdelaziz, R.F., Thomas, A.M., Raju, L.L., Khan, S.S., 2022. A prominent dual heterojunction framed CuWO4/Bi2WO6/MnS ternary NCs for para-chlorophenol degradation, Cr(VI) reduction & toxicity studies. Chemosphere 302, 134802. https://doi.org/10.1016/j.chemosphere.2022.134802.

Sumpter, J.P., Margiotta-Casaluci, L., 2022. Environmental occurrence and predicted pharmacological risk to freshwater fish of over 200 neuroactive pharmaceuticals in widespread use. Toxics 10, 233. https://doi.org/10.3390/toxics10050233.

Sun, K., Zhou, H., Li, X., Ma, X., Zhang, D., Li, M., 2022. The novel 2-dimensional Bi2MoO6-Bi2O3-Ag3PO4 ternary photocatalyst with n-n-p heterojunction for enhanced degradation performance. J. Alloys Compd. 913, 165119. https://doi.org/10.1016/j.jallcom.2022.165119.

Tahir, N., Zahid, M., Bhatti, I.A., Jamil, Y., 2022. Fabrication of visible light active Mn-doped Bi2WO6-GO/MoS2 heterostructure for enhanced photocatalytic degradation of methylene blue. Environ. Sci. Pollut. Control Ser. https://doi.org/10.1007/s11356-021-16094-5.

Tang, G., Zhang, F., Huo, P., Zulfiqarc, S., Xu, J., Yan, Y., Tang, H., 2019. Constructing novel visible-light-driven ternary photocatalyst of AgBr nanoparticles decorated 2D/2D heterojunction of g-C3N4/BiOBr nanosheets with remarkably enhanced photocatalytic activity for water-treatment. Ceram. Int. 45, 19197–19205. https://doi.org/10.1016/j.ceramint.2019.06.167.

Tayebi, M., Lee, B.K., 2019. Recent advances in BiVO4 semiconductor materials for hydrogen production using photoelectrochemical water splitting. Renew. Sustain. Energy Rev. 111, 332–343. https://doi.org/10.1016/j.rser.2019.05.030.

Wang, H., Li, X., Zhao, X., Li, C., Song, X., Zhang, P., Huo, P., Li, X., 2022. A review on heterogeneous photocatalysis for environmental remediation: from semiconductors to modification strategies. Chinese J. Catal. 43, 178–214. https://doi.org/10.1016/S1872-2067(21)63910-4.

Wang, H., Wang, J., Xiang, X., Zhou, Y., Li, Q., Tang, A., Liao, D., Liu, Y., Liu, H. bo, 2020. Preparation of PVDF/CdS/Bi2WO6/ZnO hybrid membrane with enhanced visible-light photocatalytic activity for degrading nitrite in water. Environ. Res. 191, 110036. https://doi.org/10.1016/j.envres.2020.110036.

Wang, H., Zhang, L., Chen, Z., Hu, J., Li, S., Wang, Z., Liu, J., Wang, X., 2014. Semiconductor heterojunction photocatalysts: design, construction, and photocatalytic performances. Chem. Soc. Rev. 43, 5234. https://doi.org/10.1039/C4CS00126E.

Wang, J., Lin, W., Dong, M., Xing, Y., Zhang, Q., 2021. Facile synthesize of CdS QDs decorated Bi 2 MoO 6/Bi 2 Mo 3 O 12 heterojunction photocatalysts and enhanced performance of visible light removal of organic pollutants. Environ. Technol. 42, 3581–3594. https://doi.org/10.1080/09593330.2020.1737243.

Wang, L., Li, H., Zhang, S., Long, Y., Li, L., Zheng, Z., Wu, S., Zhou, L., Hei, Y., Luo, L., Jiang, F., 2020. One-step synthesis of Bi4Ti3O12/Bi2O3/Bi12TiO20 spherical ternary heterojunctions with enhanced photocatalytic properties via sol-gel method. Solid State Sci. 100, 106098. https://doi.org/10.1016/j.solidstatesciences.2019.106098.

Wang, L., Zhu, B., Zhang, J., Ghasemi, J.B., Mousavi, M., Yu, J., 2022. S-scheme heterojunction photocatalysts for CO2 reduction. Matter 5, 4187–4211. https://doi.org/10.1016/j.matt.2022.09.009.

Wang, M., Zhang, Y., Jin, C., Li, Z., Chai, T., Zhu, T., 2019. Fabrication of novel ternary heterojunctions of Pd/g-C3N4/Bi2MoO6 hollow microspheres for enhanced visible-light photocatalytic performance toward organic pollutant degradation. Sep. Purif. Technol. 211, 1–9. https://doi.org/10.1016/j.seppur.2018.09.061.

Wang, N., Wang, W., Qi, D., Kang, G., Wang, B., Zhang, H., Ruan, J., Lei, R., Zhang, Z., Zhang, S., Zhou, H., 2024. Development of efficient and economic Bi2O3/BN/Co3O4 composite photocatalyst: Degradation mechanism, pathway and toxicity study of norfloxacin. Chemosphere 352, 141481. https://doi.org/10.1016/j.chemosphere.2024.141481.

Wang, Q., Ren, C., Zhao, Y., Fang, F., Yin, Y., Ye, Y., Yang, K., Yang, Q., Wang, K., 2023. Photocatalytic pollutant elimination and hydrogen production over TiO2 NTs/Bi2S3-MoS2 with Z-scheme configuration: kinetics and mechanism. Mater. Res. Bull. 167, 112430. https://doi.org/10.1016/j.materresbull.2023.112430.

Wang, R., Zhu, P., Duan, M., Xu, J., Liu, M., Luo, D., 2021. Synthesis and characterization of successive Z-scheme CdS/Bi2MoO6/BiOBr heterojunction photocatalyst with efficient performance for antibiotic degradation. J. Alloys Compd. 870, 159385. https://doi.org/10.1016/j.jallcom.2021.159385.

Wang, S., Zhao, L., Gao, L., Yang, D., Wen, S., Huang, W., Sun, Z., Guo, J., Jiang, X., Lu, C., 2022. Fabrication of ternary dual Z-Scheme AgI/ZnIn2S4/BiVO4 heterojunction photocatalyst with enhanced photocatalytic degradation of tetracycline under visible light. Arab. J. Chem. 15, 104159. https://doi.org/10.1016/j.arabjc.2022.104159.

Wang, W., Wang, X., Li, G., Wu, X., Yu, Q., Wang, Y., Zhao, X., Gao, J., Wang, J., 2025. Exquisitely designed (0 0 1) active face of Bi2O2CO3 based on Bi3O4Br/g-C3N5 layers with multi-channel charge transfer for efficient purification of organic water pollutants under visible light. J. Colloid Interface Sci. 690, 137297. https://doi.org/10.1016/j.jcis.2025.137297.

Wang, Yile, Yu, D., Wang, W., Gao, P., Zhong, S., Zhang, L., Zhao, Q., Liu, B., 2020. Synthesizing Co3O4-BiVO4/g-C3N4 heterojunction composites for superior photocatalytic redox activity. Sep. Purif. Technol. 239, 116562. https://doi.org/10.1016/j.seppur.2020.116562.

Wang, Yazhou, Zu, M., Zhou, X., Lin, H., Peng, F., Zhang, S., 2020. Designing efficient TiO2-based photoelectrocatalysis systems for chemical engineering and sensing. Chem. Eng. J. 381, 122605. https://doi.org/10.1016/j.cej.2019.122605.

Wang, Z., Huang, X., Wang, X., 2019. Recent progresses in the design of BiVO4-based photocatalysts for efficient solar water splitting. Catal. Today 335, 31–38. https://doi.org/10.1016/j.cattod.2019.01.067.

Wang, Z., Li, J., Fu, S., Guo, D., Tang, J., Yang, X., Xu, R., Sui, G., Chen, S., 2023. Construction of MoS2/CdS/Bi2MoO6 Z-scheme photocatalyst for efficient photocatalytic degradation under visible-light. J. Solid State Chem. 322. https://doi.org/10.1016/j.jssc.2023.123957.

Wang, Z. xu, Zhu, wen, X., Chen, C. hong, Yang, M., Yu, H., Dong, X. ting, Yang, Y., 2025. Bi-QDs modified β-Bi2O3/BiOCl ternary bismuth series photocatalyst and its photocatalytic properties. J. Solid State Chem. 345, 125225. https://doi.org/10.1016/j.jssc.2025.125225.

WHO, UNICEF, World Bank, 2022. State of the world's drinking water : an urgent call to action to accelerate progress on ensuring safe drinking water for all. World Heal. Organ. 114.

Wu, S., Guo, J., Wang, Y., 2020. Bi2O2CO3–Bi2O2(OH)NO3/g-C3N4 heterojunction as a visible-light-driven photocatalyst with enhanced photogenerated charge separation. J. Alloys Compd. 818, 152852. https://doi.org/10.1016/j.jallcom.2019.152852.

Wu, Y., Yin, Y., Su, X., Liu, W., Yi, G., Shi, S., Oderinde, O., Zeng, H., Xiao, G., Zhang, C., Zhang, Y., 2024a. GO/Bi2O2CO3/NiWO4 with Z-scheme heterojunction: efficiently enhanced degradation of organic pollutants under visible light and DFT studies. Process Saf. Environ. Prot. 190, 173–185. https://doi.org/10.1016/j.psep.2024.07.021.

Wu, Y., Yin, Y., Su, X., Yi, G., Shi, S., Oderinde, O., Xiao, G., Zhang, C., Zhang, Y., 2024b. Efficiently enhanced degradation for the organic pollutants over GO/BiOI/NiWO4 with Z-scheme heterojunction and DFT studies. J. Environ. Chem. Eng. 12, 113609. https://doi.org/10.1016/j.jece.2024.113609.

Xie, J., situ, W., Wang, R., Ni, Z., Li, Y., Ye, S., Song, X., 2022. The visible light photocatalytic degradation of ethylene using a polyvinyl alcohol film loaded with Ag2O-TiO2-Bi2WO6 heterojunction microspheres. Appl. Surf. Sci. 584, 152562. https://doi.org/10.1016/j.apsusc.2022.152562.

Xie, J., Xu, M., Wang, R., Ye, S., Song, X., 2021. Three-dimensional porous spherical TiO2–Bi2WO6 decorated graphene oxide nanosheets photocatalyst with excellent visible light catalytic degradation of ethylene. Ceram. Int. 47, 14183–14193. https://doi.org/10.1016/j.ceramint.2021.01.286.

Xu, Q., Zhang, L., Yu, J., Wageh, S., Al-Ghamdi, A.A., Jaroniec, M., 2018. Direct Z-scheme photocatalysts: principles, synthesis, and applications. Mater. Today 21, 1042–1063. https://doi.org/10.1016/j.mattod.2018.04.008.

Xu, Y., Ren, Y., Liu, X., Li, H., Lu, Z., 2024. NH2-UIO-66 based hydrophobic porous liquid with high mass transfer and affinity surface for enhancing CO2 photoreduction. Acta Physico-Chimica Sin. 40, 2403032. https://doi.org/10.3866/PKU.WHXB202403032.

Yin, C., Liu, Y., Lv, X., Lv, S., cheng, H., Kang, X., Li, X., 2022. Carbon dots as heterojunction transport mediators effectively enhance BiOI/g-C3N4 synergistic persulfate degradation of antibiotics. Appl. Surf. Sci. 601, 154249. https://doi.org/10.1016/j.apsusc.2022.154249.

Yin, G., Jia, Y., Lin, Y., Zhang, C., Zhu, Z., Ma, Y., 2022. A review on hierarchical Bi 2 MoO 6 nanostructures for photocatalysis applications. New J. Chem. 46, 906–918. https://doi.org/10.1039/D1NJ04705A.

Zhang, D., Yang, Z., Hao, J., Zhang, T., Sun, Q., Wang, Y., 2021. Boosted charge transfer in dual Z-scheme BiVO4@ZnIn2S4/Bi2Sn2O7 heterojunctions: towards superior photocatalytic properties for organic pollutant degradation. Chemosphere 276, 130226. https://doi.org/10.1016/j.chemosphere.2021.130226.

Zhang, H., Zhang, Z., Tang, Y., Han, J., Wu, Z., Wei, Z., Wang, S., Cao, Y., Zhang, S., Zhang, Y., 2025. Innovative synthesis of ternary heterojunction CuInS2/BiOI/

Bi2MoO6 for 2,4-DCP degradation and its dechlorination performance. Sep. Purif. Technol. 357, 130165. https://doi.org/10.1016/j.seppur.2024.130165.
Zhang, J., Sun, X., Zhu, W., Liu, G., Xian, T., Yang, H., 2024. Design of CdZnS/BiOCl heterostructure as a highly-efficient piezo-photocatalyst for removal of antibiotic. J. Environ. Chem. Eng. 12, 114405. https://doi.org/10.1016/j.jece.2024.114405.
Zhang, J.J., Kai, C.M., Zhang, F.J., Wang, Y.R., 2022. Novel PAN/Bi2MoO6/Ti3C2 ternary composite membrane via electrospinning with enhanced photocatalytic degradation of tetracycline. Colloids Surfaces A Physicochem. Eng. Asp. 648, 129255. https://doi.org/10.1016/j.colsurfa.2022.129255.
Zhang, L., Jaroniec, M., 2018. Toward designing semiconductor-semiconductor heterojunctions for photocatalytic applications. Appl. Surf. Sci. 430, 2–17. https://doi.org/10.1016/j.apsusc.2017.07.192.
Zheng, X., Xu, M., Cai, C., Yuan, Y., Lin, F., Chen, W., Yang, F., 2024. Enhanced photocatalytic activity of BiOCl/BiOBr/SnS2 heterojunction using a superfine SnS2 and double S-scheme. J. Alloys Compd. 980, 173630. https://doi.org/10.1016/j.jallcom.2024.173630.
Zhou, C., Wei, J., Li, Yi, Lin, H., Zhou, J., Li, Ya-yun, 2025. Journal of Colloid and Interface Science Fibrous Mos 2/Bi 2 S 3/Bifeo 3 Ternary Heterojunction Boosts Piezoelectric Photocatalytic Performance, 683, pp. 380–392.
Zhou, G., Liu, X., Xu, Y., Feng, S., Lu, Z., Liu, Z., 2024a. Enhancing d/p-2π* orbitals hybridization via strain engineering for efficient CO 2 photoreduction. Angew. Chemie Int. Ed. 63, e202411794. https://doi.org/10.1002/anie.202411794.
Zhou, G., Xu, Y., Cheng, Y., Yu, Z., Wei, B., Liu, X., Chen, Z., Li, C., Lu, Z., 2023. Rapid dissociation of high concentration excitons between [Bi2O2]2+ slabs with multifunctional N-Bi-O sites for selective photoconversion into CO. Appl. Catal. B Environ. 335, 122892. https://doi.org/10.1016/j.apcatb.2023.122892.
Zhou, G., Xu, Y., Wang, P., Tang, L., Cheng, Y., Jin, J., Ma, Z., Liu, X., Li, C., Lu, Z., 2024b. Homogenization spin coating strategy for synthesizing IM-BTO photocatalytic membrane aims to tetracycline selectively degradation. Chem. Eng. J. 486, 150163. https://doi.org/10.1016/j.cej.2024.150163.
Zhou, Y., Zhang, J., Wu, D., 2022. Enhanced photocatalytic degradation of ciprofloxacin over Bi2MoO6/g-C3N4/BiFeO3 heterojunction photocatalyst under visible light irradiation. Mater. Sci. Semicond. Process. 151, 107011. https://doi.org/10.1016/j.mssp.2022.107011.
Zhu, P., Luo, D., Liu, M., Duan, M., Lin, J., Wu, X., 2022. Flower-globular BiOI/BiVO4/g-C3N4 with a dual Z-scheme heterojunction for highly efficient degradation of antibiotics under visible light. Sep. Purif. Technol. 297, 121503. https://doi.org/10.1016/j.seppur.2022.121503.
Zulfa, L.L., Oktavianti, N.I., Hidayat, A.R.P., Utomo, W.P., Putri, D.R., Hartanto, D., Widyastuti, Ediati, R., 2024. Recent advances of CDs-based ternary heterojunctions for enhancing photocatalytic performance in the degradation of organic pollutants: a review. Nano-Struct. Nano-Objects 37, 101104. https://doi.org/10.1016/j.nanoso.2024.101104.